คุณลักษณะและสมบัติของตัวเร่งปฏิกิริยาแพลเลเดียมบนตัวรองรับไทเทเนียที่เติมไนโตรเจนในปฏิกิริยาไฮโดรจิเนชันแบบเลือกเกิดของหนึ่งเฮปไทน์

นางสาวศิวพร เพ็ชรทองช่วย

วิทยานิพนธ์นี้เป็นส่วนหนึ่งของการศึกษาตามหลักสูตรปริญญาวิศวกรรมศาสตรมหาบัณฑิต
สาขาวิชาวิศวกรรมเคมี ภาควิชาวิศวกรรมเคมี
คณะวิศวกรรมศาสตร์ จุฬาลงกรณ์มหาวิทยาลัย
ปีการศึกษา 2556
ลิขสิทธิ์ของจุฬาลงกรณ์มหาวิทยาลัย

CHARACTERISTICS AND CATALYTIC PROPERTIES OF Pd CATALYSTS SUPPORTED ON N-DOPED TiO_2 IN SELECTIVE HYDROGENATION OF 1-HEPTYNE

Miss Siwaporn Phetthongchuai

A Thesis Submitted in Partial Fulfillment of the Requirements
for the Degree of Master of Engineering Program in Chemical Engineering
Department of Chemical Engineering
Faculty of Engineering
Chulalongkorn University
Academic Year 2013

Thesis Title	CHARACTERISTICS AND CATALYTIC PROPERTIES OF Pd CATALYSTS SUPPORTED ON N-DOPED TiO_2 IN SELECTIVE HYDROGENATION OF 1-HEPTYNE
By	Miss Siwaporn Phetthongchuai
Field of Study	Chemical Engineering
Thesis Advisor	Associate Professor Dr. Joongjai Panpranot, Ph.D.

Accepted by the Faculty of Engineering, Chulalongkorn University in Partial Fulfillment of the Requirements for the Master's Degree

.....Dean of the Faculty of Engineering

(Professor Bundhit Eua-arporn, Ph.D.)

THESIS COMMITTEE

.....Chairman

(Associate Professor Dr. Bunjerd Jongsomjit, Ph.D.)

.....Thesis Advisor

(Associate Professor Dr. Joongjai Panpranot, Ph.D.)

.....Examiner

(Assistant Professor Dr. Suphot Phatanasri, Ph.D.)

.....External Examiner

(Assistant Professor Dr. Okorn Mekasuwandamrong, D.Eng.)

ศิวพร เพ็ชรทองช่วย : คุณลักษณะและสมบัติของตัวเร่งปฏิกิริยาแพลเลเดียมบนตัวรองรับไทเทเนียที่เติมไนโตรเจนในปฏิกิริยาไฮโดรจิเนชันแบบเลือกเกิดของหนึ่งเฮปไทน์. (CHARACTERISTICS AND CATALYTIC PROPERTIES OF Pd CATALYSTS SUPPORTED ON N-DOPED TiO_2 IN SELECTIVE HYDROGENATION OF 1-HEPTYNE) อ.ที่ปรึกษาวิทยานิพนธ์หลัก: รศ. ดร. จูงใจ ปั้นประณต , 72 หน้า.

ศึกษาคุณลักษณะและสมบัติของตัวเร่งปฏิกิริยาแพลเลเดียมบนตัวรองรับไทเทเนียที่ปรับปรุงด้วยไนโตรเจนในปฏิกิริยาไฮโดรจิเนชันของหนึ่งเฮปไทน์ในวัฏภาคของเหลว โดยเตรียมตัวรองรับไทเทเนียด้วยวิธีโซลเจลและใช้สารละลายนอร์มอลเมทิลไพโรริโดนเป็นแหล่งของไนโตรเจน โดยศึกษาผลของอุณหภูมิที่ใช้เผาและปริมาณสารละลายนอร์มอลเมทิลไพโรริโดน จากการวิเคราะห์คุณลักษณะของตัวเร่งปฏิกิริยาด้วยเอ็กซเรย์ดิฟแฟรกชัน การดูดซับทางกายภาพด้วยแก๊สไนโตรเจน เอ็กซเรย์โฟโตอิเล็กตรอนสเปกโทรสโคปี ฟูเรียร์ทรานฟอร์มอินฟราเรดสเปกโทรสโคปี ยูวี-วิสิเบิลสเปกโทรโฟโตมิเตอร์ กล้องจุลทรรศน์อิเล็กตรอนแบบส่องผ่าน และการดูดซับทางเคมีด้วยแก๊สไฮโดรเจน พบว่าตัวเร่งปฏิกิริยาแพลเลเดียมบนตัวรองรับไทเทเนียที่ปรับปรุงด้วยไนโตรเจน ให้ค่าความว่องไวในการเกิดปฏิกิริยาสูงกว่าตัวเร่งปฏิกิริยาแพลเลเดียมบนตัวรองรับไทเทเนียที่ไม่มีการปรับปรุง โดยตัวเร่งปฏิกิริยาแพลเลเดียมบนตัวรองรับไทเทเนียที่เติมไนโตรเจนปริมาณ 20 มิลลิลิตร และเผาที่อุณหภูมิ 300 องศาเซลเซียส แสดงประสิทธิภาพของตัวเร่งปฏิกิริยาที่ดีที่สุดคือ มีค่าความสามารถในการเลือกเกิดเป็นเฮปทีนสูงที่สุดเมื่อหนึ่งเฮปไทน์เปลี่ยนไปเป็นผลิตภัณฑ์อย่างสมบูรณ์ การเติมไนโตรเจนบนตัวรองรับไทเทเนีย ส่งผลให้พื้นที่ผิวเพิ่มขึ้น ขนาดอนุภาคของแพลเลเดียมมีขนาดเล็กลง จำนวนของแพลเลเดียมที่เป็นแหล่งกัมมันต์เพิ่มขึ้น การกระจายตัวของแพลเลเดียมเพิ่มขึ้น และเกิดอันตรกิริยาของโลหะกับตัวรองรับที่แข็งแรงขึ้น

ภาควิชา วิศวกรรมเคมี ลายมือชื่อนิสิต .....

สาขาวิชา วิศวกรรมเคมี ลายมือชื่อ อ.ที่ปรึกษาวิทยานิพนธ์หลัก .....

ปีการศึกษา 2556

5570404221 : MAJOR CHEMICAL ENGINEERING
KEYWORDS: SOL-GEL METHOD / PD CATALYST / N-DOPED TIO2 / LIQUID PHASE HYDROGENATION

SIWAPORN PHETTHONGCHUAI: CHARACTERISTICS AND CATALYTIC PROPERTIES OF Pd CATALYSTS SUPPORTED ON N-DOPED TiO_2 IN SELECTIVE HYDROGENATION OF 1-HEPTYNE. ADVISOR: ASSOC. PROF. DR. JOONGJAI PANPRANOT, Ph.D., 72 pp.

Characteristics and catalytic properties of the Pd/N-doped TiO_2 catalysts were studied in the liquid-phase hydrogenation of 1-heptyne. The TiO_2 support was prepared by sol-gel method using N-metylprrolidone (NMP) solution as the nitrogen source. The effects of calcination temperature and the amount of nitrogen doping on TiO_2 supports were investigated. The catalysts were characterized by XRD, N_2 physisorption, XPS, FT-IR, UV-vis, TEM and H_2 chemisorption. The results showed that the Pd catalysts supported on N-doped TiO_2 supports exhibited higher activity than the Pd catalysts supported on the non-modified TiO_2 support. The catalyst prepared on the TiO_2 supported that was modified with NMP of 20 ml and calcined at 300^{o}C exhibited the best catalyst performance, in which high heptane selectivity (~90%) was obtained at complete conversion of 1-heptyne. The use of N-doped TiO_2 resulted in larger catalyst surface area, smaller Pd paticles, higher amounts of Pd active sites, higher Pd dispersion and stronger metal-support interaction.

Department: Chemical Engineering Student's Signature .....

Field of Study: Chemical Engineering Advisor's Signature .....

Academic Year: 2013

ACKNOWLEDGEMENTS

This thesis would successfully completed in a short time with the kindness from my thesis advisor, Assoc. Prof. Dr. Joongjai Panpranot for suggestions, encouragement and all her help throughout the duration of this research.

In addition, the thesis author would like to grateful for his guidance, Asst. Prof. Dr. Okorn Mekasuwandamrong from Department of Chemical Engineering, Silpakorn University and also be cooperated in the external examiner. And I extremely honored to Assoc. Prof. Dr. Bunjerd Jongsomjit as the chairman and Asst. Prof. Dr. Suphot Phatanasri as the examiner.

Moreover, I would like to thank all those who have helped, supported and encouraged in this research, especially research assistants, all my friends and my parents.

Finally, this research was financially supported by the Thailand Research Fund, Office of Higher Education Commission and Chulalongkorn University (Advanced Materials Cluster).

CONTENTS

Page

Page

TABLES CONTENT

Page

FIGURES CONTENT

Page

Page

CHAPTER 1

INTRODUCTION

1.1 General introduction

The selective hydrogenation of alkynes to alkenes is an important step in fine chemicals production and industrial polymerization processes with the aim of the complete elimination of alkynes from alkene feedstocks [1, 2]. Alkyne compounds, such as 1-hexyne [3, 4], 3-hexyne [5], 1-heptyne [6-9], 4-octyne [10], phenylacetylene [11, 12], and 1-phenyl-1-pentyne [13], have been employed as model reactants for evaluation of the liquid-phase selective hydrogenation catalysts under mild reaction conditions. Noble metals (Pd [14, 15], Pt [16], Rh [17, 18], and Ru [2, 19]) have been widely used for hydrogenation reaction because they adsorb hydrogen with dissociation and the bonding is not too strong. Moreover, the advantages of noble metal catalysts are their relatively high activity, easiness to separation and mild reaction conditions [5, 7, 20].

Palladium is one of the most important hydrogenation catalysts used in industries and studied in fundamental research [21] due to some sort of structure sensitivity of palladium catalysts in alkyne hydrogenation [22-25], which is in strong contrast to the accepted structure insensitivity of hydrogenation. Furthermore, it is able to selectively hydrogenate more alkynes than alkenes [15, 26].

In recent years, supported palladium catalysts was used in the selective hydrogenation of alkyne to alkene such as propyne to propene [9], butadiene to butene [27], 3-methyl-1-pentyn-3-ol to 3-methyl-1-penten-3-ol [28], pentyne to pentene [29] and 1-heptyne to heptene [30]. The activity and selectivity of palladium catalysts in the selective hydrogenation reaction depend on interaction between the support and palladium catalysts. Several support materials, such as CeO_2 [27], ZnO [27], SiO_2 [28, 31], Al_2O_3 [29, 30] and TiO_2 [9, 27, 31, 32] have been applied for palladium catalysts to study the effect of support on the activity and selectivity of hydrogenation.

Recently, TiO_2 has received much attention in selective hydrogenation reaction. Strong metal-support interaction has associated with noble metal supported on reduced oxides, which shows important differences in the catalytic activity and selectivity of hydrogenation reaction when compared between reduction at low temperature and high temperature [31]. Anatase titania supported palladium catalyst pre-reduced at lower temperature has higher selectivity of alkene for the liquid phase selective hydrogenation of long chain alkadienes than rutile titania supported palladium catalysts [32].

In photocatalysis, the synthesized N-doped rutile TiO_2 showed excellent photocatalytic activity in sunlight in the using methylene blue degradation, compared to the commercial rutile sample [33]. Moreover, polymorphic titania nanoparticles, prepared by post-treated by a solvent-based ambient condition sol (SACS) process in sec-butanol have shown improved photocatalytic activity. The increase in the surface area of SACS samples is not the main factor for the improvement of photocatalytic activity, but the main factor is due to less lattice hydroxyl content. Moreover, all prepared polymorphic titania samples showed excellent photocatalytic activity in methyl orange degradation under UV when compared to commercial P25 [34]. It is interesting to study the use of N-doped TiO_2 as Pd catalyst support for the selective hydrogenation.

The approach introduced in this study is to synthesize N-doped TiO_2 by a sol-gel method using N-methylpyrolidone (NMP) as the nitrogen source with various amounts of NMP and employed as Pd catalyst supports. The liquid phase hydrogenation of heptyne is carried out as the reaction test for those catalysts. The properties of the catalysts are also characterized by various techniques.

1.2 Research objectives

To investigate the characteristics and catalytic properties of the N-doped TiO_2 supported Pd catalysts in the liquid-phase selective hydrogenation of 1-heptyne to 1-heptene.

1.3 Research scopes

1) Synthesis of the TiO_2 supports by using the sol-gel method.

2) Synthesis of the N-doped TiO_2 supports by using NMP solution as the nitrogen source with and without calcinations and constant amounts of NMP solution

3) Synthesis of the N-doped TiO_2 supports by using NMP as the nitrogen source with various amounts of NMP solution and constant calcination temperature.

4) Synthesis of the Pd/TiO_2 and the Pd/N-doped TiO_2 catalysts by using the wet impregnation method with 1 M HCl solution and the palladium content of 0.5% wt.

5) Catalyst calcination in air at 450°C for 3 h and followed by reduction in H_2 flow at 40°C for 2 h.

6) Reaction study of the Pd/TiO_2 and the Pd/N-doped TiO_2 catalysts in the liquid-phase selective hydrogenation of 1-heptyne to 1-heptene by using the stirred batch reactor under H_2 pressure of 0.2 MPa and temperature of 30°C for 10, 30, 60 and 120 min.

7) Characterization of the TiO_2 support, the N-doped TiO_2 supports, the Pd/TiO_2 and the Pd/N-doped TiO_2 catalysts by using various techniques:

- X-ray diffraction (XRD)
- N_2 physisorption
- X-ray photoelectron spectroscopy (XPS)
- UV-vis spectrophotometer (UV-vis)
- Fourier transform infrared spectroscopy (FT-IR)
- Transmission electron microscopy (TEM)
- H_2 chemisorption

1.4 Research methodology

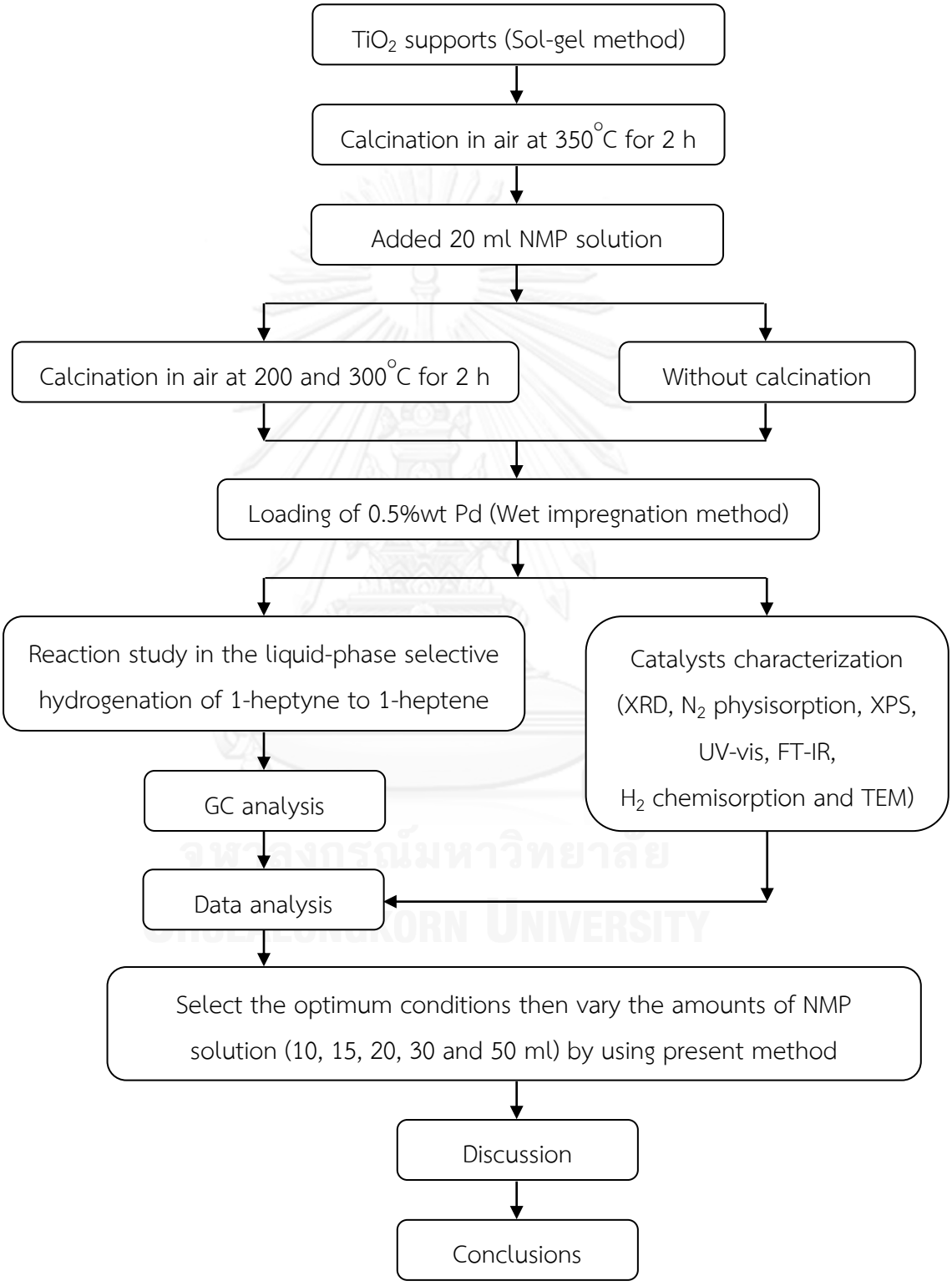

CHAPTER 2

THEORY AND LITERATURE REVIEWS

2.1 Hydrogenation reaction

Hydrogenation is the addition of hydrogen to a carbon-carbon multiple bond. Alkyne hydrogenation process has been widely used in industry to purify olefin streams and comprises a prototype reaction to understand selectivity in heterogeneous catalyzed reactions, which consists of two phases, a solvent and a metal. A solvent used in catalytic hydrogenation reaction, such as ethanol, hexane, acetic acid or toluene, is chosen by its ability to dissolve the alkyne and is usually present to influence product selectivity and to adsorb the reaction heat liberated by the reaction. Since most hydrogenations are highly exothermic, careful temperature control is required to achieve the desired selectivity and to prevent temperature runaway. Metal catalysts widely used are Pd [3, 4], Pt [5], Rh [6, 7] and Ru [8, 9]. Pd is used especially because of its stronger adsorption of carbon-carbon triple bond on the catalytic surface compared with a carbon-carbon double bond [28] and relatively high activity [10-12].

The selective hydrogenation of alkynes is an addition of hydrogen to a carbon-carbon triple bond in order to produce only alkenes product. The overall effect of such an addition is the reductive removal of the triple bond functional group. The simplest source of two hydrogen atoms is molecular hydrogen. The complete reaction network starts by hydrogen dissociation and the adsorption of the alkyne on the surface. Both steps are exothermic under all conditions but mixing alkynes with hydrogen does not result in any discernable reaction [35]. However, addition of hydrogen to the alkene is very slow in the absence of a metal catalyst, meaning that any uncatalyzed mechanism must have very high activation energy. The mechanism of potential energy profiles for with catalysis and without catalysis shown in the following **Figure 2.1.**

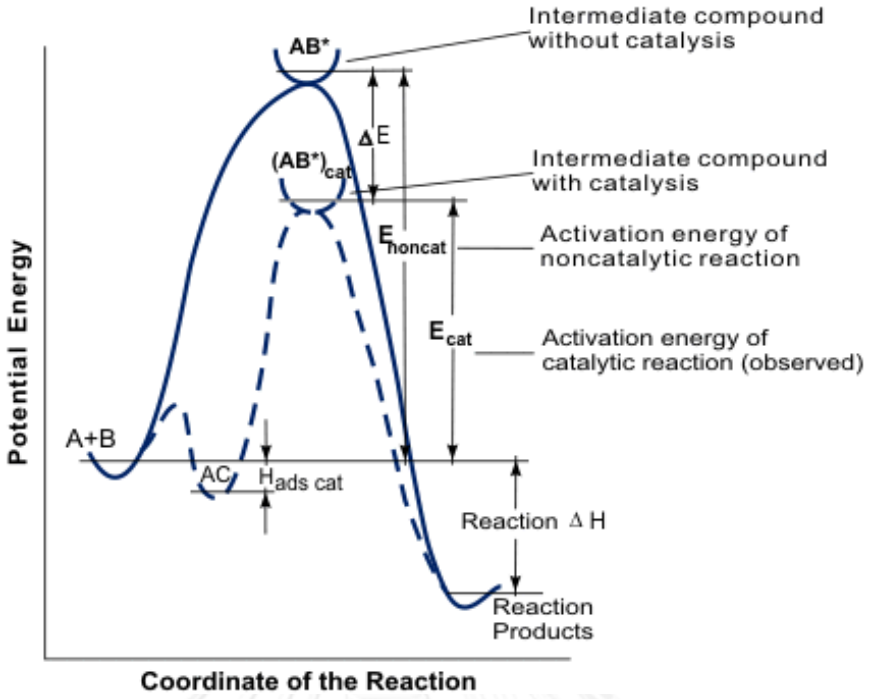

Figure 2.1 Potential energy profiles for with catalysis and without catalysis reactions [36]

The selective hydrogenation of alkynes to alkenes is the reaction which takes place on the surface of the metal catalyst. The mechanism of the reaction can be described in 4 steps [37] :

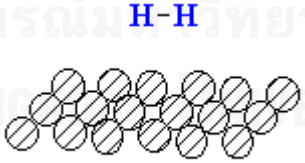

Step 1 : Hydrogen molecules react with metal atoms at the catalyst surface. The relatively strong hydrogen-hydrogen bond is broken and replaced by two weak metal-hydrogen bonds.

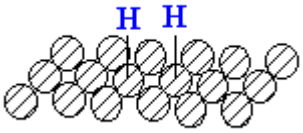

Step 2 : The alkyne reacts with the metal catalyst. The component of the carbon-carbon triple bond between the two carbons is replaced by two relatively weak carbon-metal bonds.

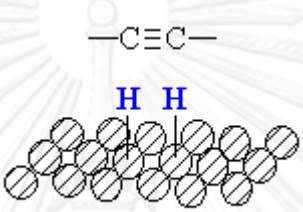

Step 3 : A hydrogen atom is transferred from the catalyst surface to one of the carbon-carbon triple bond.

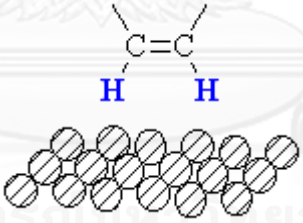

Step 4 : The second hydrogen atom is transferred, forming the alkene. The sites on the catalyst surface at which the reaction occurred are free to accept additional hydrogen and alkyne molecules.

2.2 Palladium catalyst

Palladium is one of the most important hydrogenation catalysts used in industry and studied in fundamental research [21]. The Pd catalysts have several important advantages [38] :

1) Many different metal precursors are known and available

2) The Pd forms complexes with a wide variety of organic ligands with P, N, and O atoms

3) Many of these complexes are relatively easy to prepare and to handle

4) The Pd-catalyzed reactions give reliable results and are easy to run in the ordinary equipment

5) The functional group tolerance is often very good. The list of synthetically useful transformations is now truly impressive and explains why Pd catalysis has found its place into the repertoire of so many organic chemists.

The interaction from palladium that can selectively hydrogenate carbon-carbon multiple bond to carbon-carbon double bond is attributed to the strong adsorption. According to the classical interpretation of palladium, activity and selectivity because it has strong metal-support interaction (SMSI) effect [31, 32, 39].

Mekasuwandumrong et al. [40] studied the hydrogenation rate of 1-heptyne evaluated by liquid-phase selective hydrogenation of 1-heptyne over Pd/TiO_2 catalyst synthesized by one-step flame spray pyrolysis and found that the hydrogenation rate of 1-heptyne increased when the Pd loading contents increased resulting in the better catalytic performance of the flame-made catalysts. These were suggested to be due to a stronger interaction between the Pd particles and the TiO_2 support.

The performance of TiO_2-modified Pd catalysts was reported by Kang et al. [31] for the selective hydrogenation of acetylene investigated by using a steady-state reaction test. The catalyst surface was characterized by H_2 and CO chemisorption were found that TiO_2-modified Pd catalyst reduced at $500^{\circ}C$. In this study, $Pd-Ti/SiO_2/500^{\circ}C$ was showed a higher selectivity for ethylene production than either the Pd/TiO_2 or Pd/SiO_2 catalyst. The amounts of chemisorbed H_2 and CO were significantly reduced and in particular, the adsorption of multiply coordinated CO species was suppressed on $Pd-Ti/SiO_2/500^{\circ}C$, because it shown a higher Pd dispersion and the strong metal-support interaction (SMSI) phenomenon and the same as the TiO_2 supported Pd catalyst reduced at $500^{\circ}C$.

2.3 Wet impregnation method

The wet impregnation method is one of the catalyst preparation. The principal of catalyst preparation consists of two stages. First the metal salt component is dispersed into a finely divided form on supports by impregnation (incipient wetness impregnation method and wet impregnation method), adsorption from solution, co-precipitation, or deposition, and secondly; the supported metal salt is converted to a metallic or oxide state by calcination or reduction.

Impregnation as a mean of supported catalyst preparation can be achieved by filling the pores of a support with a solution of the metal salt from which the solvent is subsequently evaporated. The catalyst is prepared by adding solution of a suitable metal salt onto the supports, which the required weight of the active component is incorporated into the support without the use of excess of solution, followed by drying and subsequent decomposition of the salt at an elevated temperature, either by calcination or reduction. This method of preparation it is essential to have an understanding of both chemical and physical properties [41].

2.4 Titanium oxide (TiO_2)

Titanium dioxide has been widely used in heterogeneous catalysis as photocatalysts, gas sensor, white pigment, corrosion protective coating and optical coating etc. and it is outstanding in improvement of catalytic reaction, which is the main driving force for surface investigations on titanium dioxide [42, 43]. Titanium dioxide exists in three crystalline forms [44, 45] :

1) Rutile phase, which tends to be more stable at high temperatures and thus is sometimes found in igneous rocks

2) Anatase phase, which tends to be more stable at lower temperatures

3) Brookite phase, which is usually found only in minerals

All three polymorphs can be readily synthesised in the laboratory and typically the metastable anatase and brookite will transform to the thermodynamically stable rutile upon calcination at temperatures exceeding ~600°C [46]. Only the rutile and anatase TiO_2 have significant role in industrial applications. However, solution-phase preparation methods for titanium dioxide generally favour the anatase structure.

A summary of the crystallographic properties rutile, anatase and brookite TiO_2 is given in **Table 2.1** [42].

Table 2.1 Crystallographic properties of rutile, anatase and brookite TiO_2

Crystal structural	Density (kg/m^3)	System	Space group	Cell parameters (nm)		
				a	b	c
Rutile	4240	Tetragonal	D^{14}_{4h}-$P4_2/mnm$	0.4584	-	0.2953
Anatase	3830	Tetragonal	D^{19}_{4a}-$I4_1/amd$	0.3758	-	0.9514
Brookite	4170	Rhombohedral	D^{15}_{2h}-Pbca	0.9166	0.5436	0.5135

The crystal structures of rutile and anatase have a belonging tetragonal structure but they are not isomorphous and brookite has a belonging rhombohedral structure, which shows in **Figure 2.2.**

Figure 2.2 Crystalline structures of titanium dioxide [47]

However, the properties of titanium dioxide are a function of the crystal structure, particle size, and morphology, and hence the properties of titanium dioxide dependent on the preparation methods of titanium dioxide. There are several methods to produce titanium dioxide, including [42] :

1) Hydrothermal method
2) Sol-gel method
3) Chemical vapor deposition (CVD) and physical vapor method (PVD)
4) Solvothermal
5) Electrochemical approaches (e.g. anodizing of Ti)
6) Solution combustion
7) Microemulsion technique
8) Micelle and inverse micelle method
9) Combustion flame-chemical vapor condensation process
10) Sonochemical reactions
11) Plasma evaporation

Among these preparation methods for titanium dioxide, the most successful are sol-gel method and hydrothermal method. The advantage of these methods relies on their ability to control the crystal structure, particle size, and morphology of titanium dioxide.

2.5 Sol-gel method

This method has a relatively long history. It started with processing of oxide materials including glass and ceramics about 30 years ago. Since then, the technology has been employed not only in preparation of oxide, but also in the preparation of non-oxide materials such as nitrides, carbides, fluorides and sulfides as well as oxynitride and oxycarbide glasses. Processing of organic-inorganic material is now a very active field of research. This has been expanded to the field of biotechnology where it applies in the research of encapsulation of enzymes, antibodies and bacteria. This technology is a versatile tool that makes it possible the production of a wide variety of metal oxide nanostructures with novel properties [42].

The sol-gel process has become a method for the preparation of titanium dioxide, since the physical and chemical characteristics of titanium dioxide such as crystal structure, particle size, and morphology can be controlled [48-50]. And it is

also a simple and easy means of synthesizing nanoparticles at ambient temperature under atmospheric pressure and this method does not require complicated set-up [51].

Titanium precursors, such as titanium alkoxide, are used as starting material for preparation methods of titanium dioxide [48, 52, 53]. For example, the metal alkoxides may be hydrolyzed (equation 1) and polycondensed (equation 2 and equation 3) to form a metal oxide gel as in the following reactions :

$$\text{M-OR} + H_2O \longrightarrow \text{M-OH} + \text{ROH} \qquad (1)$$

$$\text{M-OH} + \text{M-OR} \longrightarrow \text{M-O-M} + \text{ROH} \qquad (2)$$

$$\text{M-OH} + \text{M-OH} \longrightarrow \text{M-O-M} + H_2O \qquad (3)$$

Where M = Si, Ti, Zr, Al, etc., and R = alkyl group

The relative rates of hydrolysis and polycondensation strongly influence the structure and properties of the resulting metal oxides. Factors affecting the sol-gel process include the reactivity of metal alkoxides, pH of the reaction medium, water/ alkoxide ratio, reaction temperature, and nature of solvent and additive [54].

Many researchers have used the sol-gel method to prepare TiO_2. For example, Venkatachalam et al. [55] used the typical synthesis procedure for nanoparticles TiO_2 as follows. Titanium (IV) isopropoxide ($C_{12}H_{28}O_4Ti$), glacial acetic acid and water were mixed in a molar ratio of 1:10:350. The titanium (IV) isopropoxide of 18.6 ml was hydrolyzed using glacial acetic acid of 38.8 ml at 0°C. Then water of 395 ml was added drop wise under vigorous stirring for 1 h. Subsequently the solution was sonicated for 30 min followed by stirring for another 5 h until a clear solution of TiO_2 nanocrystals was formed. The solution was then placed in an oven at 70°C for 12 h to allow an aging process. The gel was then dried at 100°C and subsequently the catalyst was crushed into fine powder and calcined in muffle furnace at 500°C for 5 h. The size control of uniform anatase-type.

TiO_2 nanoparticles by sol-gel process from a condensed $Ti(OH)_4$ gel form hydrolysis of a Ti-TEOA complex have been studied by Sugimoto et al. [49] They found that the particles size anatase TiO_2 was increased from 5-30 nm with pH increasing from 0.6-12 by aging the $Ti(OH)_4$ gel at 140°C for 72 h. TEOA appeared to enhance the pH effect on the nucleation rate of anatase TiO_2 particles by adsorption onto their embryos, leading to a wide range of size control.

2.6 Nitrogen doping

Nitrogen can be easily introduced in the TiO_2 structure, due to its comparable atomic size with oxygen, small ionization energy and high stability [56]. In 1986, Sato reported that addition of NH_4OH in a titania sol, followed by calcinations of precipitated powder resulted in a material that exhibited a visible light response [57].

Urea has been reported as an N source for mechanical N-doping [58]. Liu et al. [59] also prepared yellow nitrogen-doped titania by sol-gel method in mild condition, with the elemental nitrogen source from ammonium carbonate. The analytical results demonstrated that all catalysts were anatase and the crystallite size of nitrogen-doped titania increased with increasing N/Ti ratio. The doping of nitrogen enlarged the specific surface and extended the absorption shoulder into the visible-light region. Photocatalytic activity of the nitrogen-doped titania catalysts was evaluated based on the photodegradation of methyl orange and 2-mercaptobenzothiazole in aqueous solution under visible-light. The group stated that the visible-light activity of nitrogen-doped titania was much higher than that of the commercial Degussa P25.

Valentin et al. [60] prepared N-doped TiO_2 samples via the sol-gel method using several nitrogen containing inorganic compounds (e.g. NH_4Cl, NH_3, N_2H_4, NH_4NO_3 and HNO_3) as nitrogen source. A solution of titanium (IV) isopropoxide in isopropylic alcohol was mixed with an aqueous solution of a nitrogen compound and kept upon constant stirring at room temperature. The solution obtained was left aging overnight at room temperature to ensure the completion of the hydrolysis. The solution was then dried at 343 K. The dried compound was heated at 773 K in the air for 1 h. They found that the best results were obtained using ammonium chloride as the

nitrogen source. The calcination influences the final properties of the material depending on the temperature and heating rate employed in the treatment. After heating in air at 773 K and at a relatively slow heating rate (5 K/min), the final material exhibited a pale yellow color and consisted of anatase structure. Structure of the N-doped TiO_2 is shown in **Figure 2.3.**

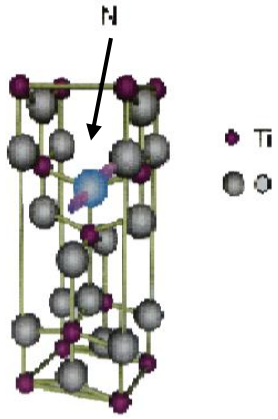

Figure 2.3 Unit cell of the N-doped anatase TiO_2 [42]

CHAPTER 3

EXPERIMENTAL

This chapter explained about the research methodology of preparation for the all supports and all the catalysts, the techniques for catalyst characterization including x-ray diffraction (XRD), N_2 physisorption, x-ray photoelectron spectroscopy (XPS), UV-vis spectrophotometer (UV-vis), fourier transform infrared spectroscopy (FT-IR), transmission electron microscopy (TEM) and H_2 chemisorption and the apparatus as used for reaction study and analysis final products.

3.1 Catalyst preparation

3.1.1 Synthesis of the supports

The supports used in this study, the TiO_2 anatase were prepared by the sol-gel method. The chemicals that used to synthesize the TiO_2 support and N-doped TiO_2 supports are shown in **Table 3.1.**

The TiO_2 supports were prepared by using the sol-gel method. First, mixture of nitric acid (7.51 ml) and deionized water (1,000 ml) in a beaker. Then, titanium (IV) isopropoxide (83.4 ml) was poured slowly and stirred continuously over time until a clear solution at room temperature. Next, The sol (clear solution) was made dialysis to adjust pH in the range 3.3 to 3.5, which was used cellulose membrane in deionized water. After that, dried in air at 110°C for 24 h to remove water and solvent and then crushed. Finally, calcinated in air at 350°C for 2 h. The resulting of the final product is TiO_2 powder.

For synthesis of the N-doped TiO_2 supports by using N-metylpyrrolidone (NMP) as the nitrogen source. First, the TiO_2 support (2 g) and NMP solution (20 ml) were added into a bottom flask in silicone oil at 170°C. Then, stirred continuously for 4 h. Next, separated solvent from supports powder by centrifugation. After that, dried in air at 110°C for 24 h. Finally, calcinated in air at 200 and 300°C for 2 h and without calcination.

Table 3.1 The chemicals used for synthesis of the TiO_2 support and N-doped TiO_2 supports

Chemicals	Supplier
Titanium (IV) isopropoxide 97%; (97% $Ti(OCH_2CH_2CH_3)_4$)	Aldrich
Nitric acid 65% (65% HNO_3)	Aldrich
N-metylpyrrolidone 99.5% (99.5% C_5H_9NO)	Merck

3.1.2 Synthesis of the Pd/TiO_2 and Pd/N-doped TiO_2 catalysts

The Pd/TiO_2 and Pd/N-doped TiO_2 catalysts were prepared by using wet impregnation method, with 0.5wt%Pd. Frist, Palladium (II) chloride (99.99% $PdCl_2$, Aldrich) that used as the Pd precursor was dissolved in 1 M of HCl solution. Then, droped to the supports (1g). Next, dried at 110°C for 24 h. Finally, calcinated in air at 450°C for 3 h to eliminate chloride contamination.

3.2 Reaction study in the liquid-phase hydrogenation of 1-heptyne

The chemicals and reagents that used in the reaction study in the liquid phase hydrogenation of 1-heptyne to heptene are shown in **Table 3.2.**

All the catalysts were evaluated by the liquid phase hydrogenation of 1-heptyne to heptane, which were carried out in magnetically stirred 50 ml of teflon container stainless steel autoclave reactor. First, all the catalysts were reduced with 50 ml/min of hydrogen gas at 40°C for 2 h. Then, the catalyst (10 mg) was dispersed in toluene (9.8 ml) which was used as an intermediate solvent and 1-heptyne (0.2 ml) at 30°C under hydrogen atmosphere of 0.2 MPa. Next, stirred continuously for 10, 30, 60 and 120 min which the schematic diagram of the liquid phase hydrogenation of 1-heptyne to heptane is shown in **Figure 3.1.**

Table 3.2 The chemicals and reagents are used in the reaction study

Chemicals and reagents	Supplier
High purity grade hydrogen (99.99%)	Thai industrial gases limited
1-Heptyne	Aldrich
1-Heptene	Merck
1-Heptane	Wako
Toluene	Merck

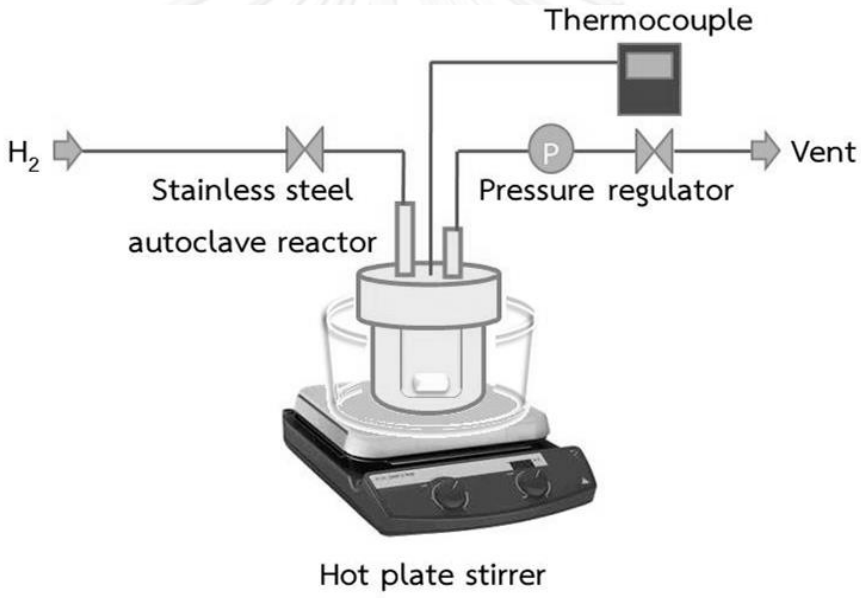

Figure 3.1 The schematic diagram of the liquid-phase hydrogenation

After that, separated final products from the catalyst by centrifugation. Finally, the final products were analyzed by gas chromatography with flame ionization detector which the operating conditions are shown in **Table 3.3.**

Table 3.3 The operating conditions for gas chromatograph

Gas chromatography	Shimadzu GC-14A
Detector	FID
Packed column	GS-alumina (length=30m, I.D.=0.53mm)
Carrier gas	Helium (99.99%)
Make-up gas	Nitrogen (99.99%)
Column temperature	190°C
Injector temperature	250°C
Detector temperature	280°C
Time analysis	10 min

3.3 Catalyst characterization

3.3.1 X-ray diffraction (XRD)

The x-ray diffraction (XRD) patterns of all the supports and all the catalysts were determined by using the SIEMENS D5000 x-ray diffractometer connected with a computer with Diffract ZT version 3.3 programs for fully control of the XRD analyzer. The experiments were carried out by using Cu K_α radiation with Ni filter in the 2θ range of 20° to 80° and resolution 0.04°.

3.3.2 N_2 physisorption

The specific surface area (using the stand BET method), average pore volume, average pore size (using the BJH desorption analysis) and hyteresis loop (using the adsorption-desorption isotherms) of all the catalysts and TiO_2 support were measured by using the Micromeritics Pulse ChemiSorb 2750 instrument. Prior to analysis, all the catalysts and TiO_2 support were thermally treated at 150ºC for 1 h. Then, nitrogen adsorption-desorption isotherms were obtained at -196ºC under liquid nitrogen.

3.3.3 X-ray photoelectron spectroscopy (XPS)

The XPS spectra, the blinding energy, full width at half maximum (FWHM) and the composition of the Pd catalysts on the surface layer of all the catalysts were performed by using the Kratos Amicus x-ray photoelectron spectroscopy. The experiment was operated with the x-ray source at 20 mA and 12 kV (240 W), the resolution at 0.1 eV/step and the pass energy of the analyzer was set at 75 eV under pressure approximately $1x10^{-6}$ Pa. For calibration, the blinding energy was referenced to C 1s line at 285.0 eV.

3.3.4 UV-vis spectrophotometer (UV-vis)

The absorbance spectrums of all the supports were recorded by using the Perkin Elmer Lambda 650 spectrophotometer in the wavelength range from 200-700 nm.

3.3.5 Fourier transform infrared spectroscopy (FT-IR)

The FT-IR spectra of all the supports were recorded by using the Nicole 6700 of the IR spectrometer in the wavelength range from 500-4000 cm^{-1}.

3.3.6 Transmission electron microscopy (TEM)

The Pd particles size and particles size distribution of all the catalysts were observed by using the JEOL-JEM 200CX transmission electron microscope operated at 200 kV at faculty of engineering, chulalongkorn university.

3.3.7 H_2 chemisorption

The amounts of H_2 chemisorption of all the catalysts for calcination of the Pd active site, %Pd dispersion and average Pd^{O} particle size was recorded by using the Micromeritics Pulse ChemiSorb 2700 instrument. Prior to the H_2 chemisorption, all the catalysts were reduced with 50 ml/min of H_2 at $40^{\circ}C$ for 2 h. Then, cooled to room temperature. Next, subjected to H_2 chemisorption using a pulse 100 µl. Finally, repeated unit the signal area was constant.

CHAPTER 4

RESULTS AND DISCUSSION

This chapter describes the details about the characteristics and catalytic properties of the Pd catalysts supported on N-doped TiO_2 supports in the selective hydrogenation of 1-heptyne. The effects of calcination temperature of the N-doped TiO_2 supports for the Pd catalysts supported on N-doped TiO_2 supports and the amount of nitrogen doping on TiO_2 supports for the Pd catalysts supported on N-doped TiO_2 supports were investigated.

4.1 The effect of calcination temperature of the N-doped TiO_2 supports

The TiO_2 support was prepared by sol-gel method. The TiO_2 support was labeled as T. The N-doped TiO_2 supports were synthesized by using N-metylpyrrolidone (NMP) solution as a nitrogen source. The NMP solution (20 ml) and the TiO_2 supports (2 g) were added into a flask in silicone oil with mixed continuously and heated at 170°C for 4 h then dried in air overnight at 110°C followed by without and with the calcinations in air at 200 and 300°C for 2 h. The N-doped TiO_2 supports were labeled as N20T, N20T200 and N20T300, respectively. All the catalysts were prepared by wet impregnation method using $PdCl_2$ as a Pd precursor with loading 0.5%wt Pd and calcined in air at 450°C for 3 h to eliminate chloride contamination. The catalysts were labeled as Pd/T, Pd/N20T, Pd/N20T200 and Pd/N20T300, respectively.

4.1.1 Catalysts characterization

4.1.1.1 X-ray diffraction (XRD)

Phase identification of the supports and the catalysts were based on the results from x-ray diffraction analysis.

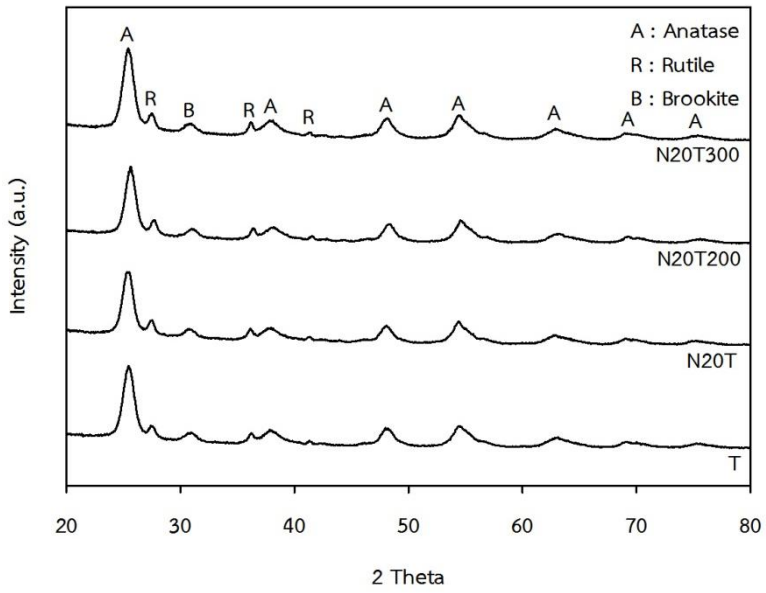

Figure 4.1 XRD patterns of the N-doped TiO_2 supports with different calcination temperatures compared with TiO_2 support

The XRD patterns of the N-doped TiO_2 supports with different calcination temperatures compared with the TiO_2 supports are shown in **Figure 4.1.** All the supports exhibited XRD characteristic peaks at 25° (the major of anatase phase), 36°, 49°, 54°, 63°, 69° and 75° 2 theta with small amounts of rutile phase appeared at 28°, 36° and 41° 2 theta and brookite phase at 31° 2 theta. The rutile phase content increased in the order N20T300 > N20T > N20T200. For the TiO_2 support, the major anatase phase was observed and the rutile phase content was higher than N20T and N20T200 but lower than N20T300.

Figure 4.2 shows the XRD characteristic peaks of the Pd catalysts supported on N-doped TiO_2 supports with different calcination temperatures compared with the Pd catalysts supported on TiO_2 support. The major of anatase phase was observed at 25°, 36°, 49°, 54°, 63°, 69° and 75° 2 theta with small amounts of rutile phase appeared at 28°, 36° and 41° 2 theta and brookite phase at 31° 2 theta. For the TiO_2 support, the major anatase phase and the rutile phase were similar to **Figure 4.1.**

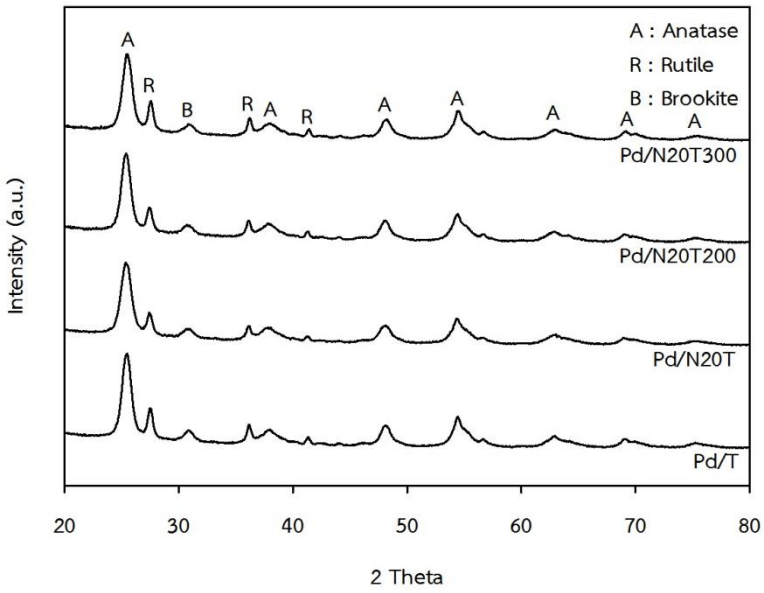

Figure 4.2 XRD patterns of the Pd catalysts supported on N-doped TiO_2 supports with different calcination temperatures compared with TiO_2 support

The peaks corresponding to the formation of PdO were not observed due to low loading the Pd catalysts content and high dispersion of the Pd catalysts supported on N-doped TiO_2 supports and TiO_2 support.

4.1.1.2 N_2 physisorption

The BET surface area, pore volume, average pore size and hyteresis loop of the titania support and the catalysts were measured by N_2 physisorption technique. **Table 4.1** shows the physical properties of the Pd catalysts supported on N-doped TiO_2 supports with different calcination temperatures and TiO_2 support. The results showed that the BET surface area of the Pd catalysts supported on TiO_2 support was lower than TiO_2 support but pore volume and average pore size were not changed. The nitrogen doping on TiO_2 support with different calcinations temperature appeared to have little effect on the BET surface area (Pd/N20T200 > Pd/N20T ~ Pd/N20T300 > Pd/T) and average pore size (Pd/N20T300 > Pd/N20T > Pd/T > Pd/N20T200). When the catalyst was without

calcination after nitrogen doping, the catalyst had a surface area of 98.6 m^2/g due to the titania surface were covered from the solvent. With calcination at 200°C presented the highest surface area (110.9 m^2/g), calcination of at this temperature only resulted in the removal of surface hydroxyls and/or organic residues [34].

Table 4.1 Physical properties of the Pd catalysts supported on N-doped TiO_2 supports with different calcination temperatures and TiO_2 support

Sample	BET surface area (m^2/g)	Pore volume (cm^3/g)	Average pore size (nm)
Pd/T	95.0	0.22	4.9
Pd/N20T	98.6	0.22	5.0
Pd/N20T200	110.9	0.20	4.8
Pd/N20T300	98.8	0.21	5.3

However, increasing the calcination temperature resulted in the surface area decrease to 98.8 m^2/g because of nitrogen atoms dislodged out with solvent. This result is similar to previous research [61]. The hyteresis loop of nitrogen adsorption-desorption isotherms consists of adsorption region and desorption region that hyteresis loop can be used predict pore characteritics of materials. The nitrogen adsorption-desorption isotherms at -196°C of the TiO_2 support, the Pd catalyst supported on TiO_2 support and Pd catalyst supported on N-doped TiO_2 supports with different calcination temperatures are shown in **Figure 4.3.** These isotherms represent to the same hyteresis loop, with the typical mesoporous structure having pore diameter ranging from 2-50 nm (IUPAC 1985 classification) [62] corresponding to data in **Table 4.1.** The TiO_2 support and all the catalysts had pore size around 4.8-5.3 nm.

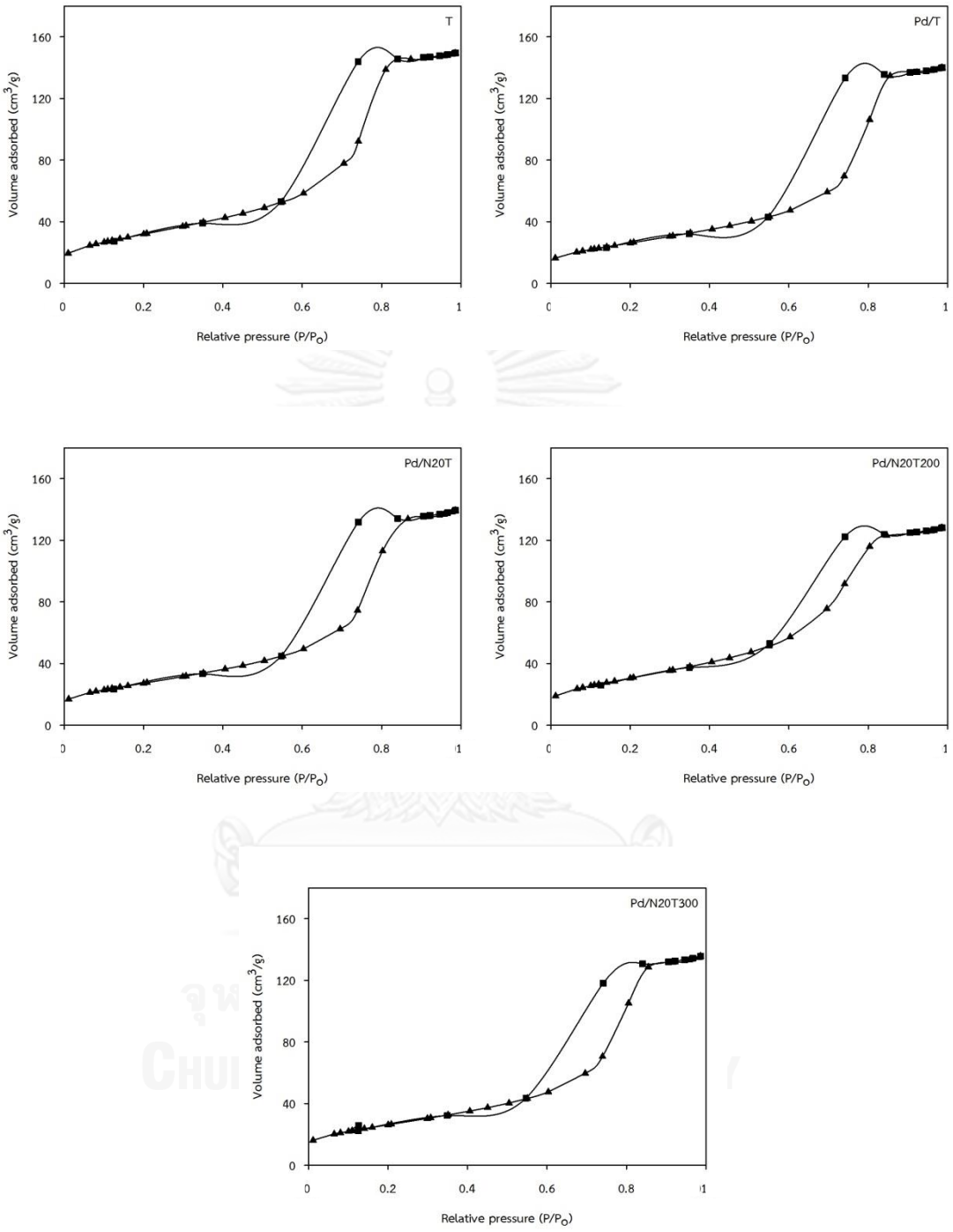

Figure 4.3 N_2 adsorption-desorption isotherms at -196°C of the TiO_2 support, the Pd catalysts supported on TiO_2 support and Pd catalysts supported on N-doped TiO_2 supports with different calcination temperatures

4.1.1.3 X-ray photoelectron spectroscopy (XPS)

The XPS analysis including XPS spectra, blinding energy, full width at half maximum (FWHM) and composition of Pd on the surface layer of the catalysts are summarized in **Table 4.2.**

The XPS spectra of the Pd 3d for the catalysts are shown in **Figure 4.4** and **Figure 4.5.** The binding energy of Pd $3d_{5/2}$ for all the catalysts were seen at binding energies around 336.5-337.5 eV. Palladium was suggested to be in the PdO form [63]. The XPS Pd 3d core level of 2%Pd/T and 2%Pd/N20T300 are shown in **Figure 4.5** that confirmed the position B.E. signal with performing by increased Pd loading from 0.5%wt to 2%wt.

The XPS peaks of N 1s for all the catalysts were not observed distinctively on Pd/N20T, Pd/N20T200 and Pd/N20T300 catalysts due to the low amount of nitrogen doping or the concentration could have been below the detection limit of the instrument.

Table 4.2 The XPS of the all catalysts

Sample	Pd 3d		
	B.E. (eV)	FWHM (eV)	Atomic concentration (%)
Pd/T	337.2	1.096	0.03
Pd/N20T	336.5	0.406	0.01
Pd/N20T200	337.5	0.709	0.03
Pd/N20T300	336.8	0.656	0.04
2%Pd/T	337.4	1.965	0.02
2%Pd/N20T300	336.9	2.704	0.03

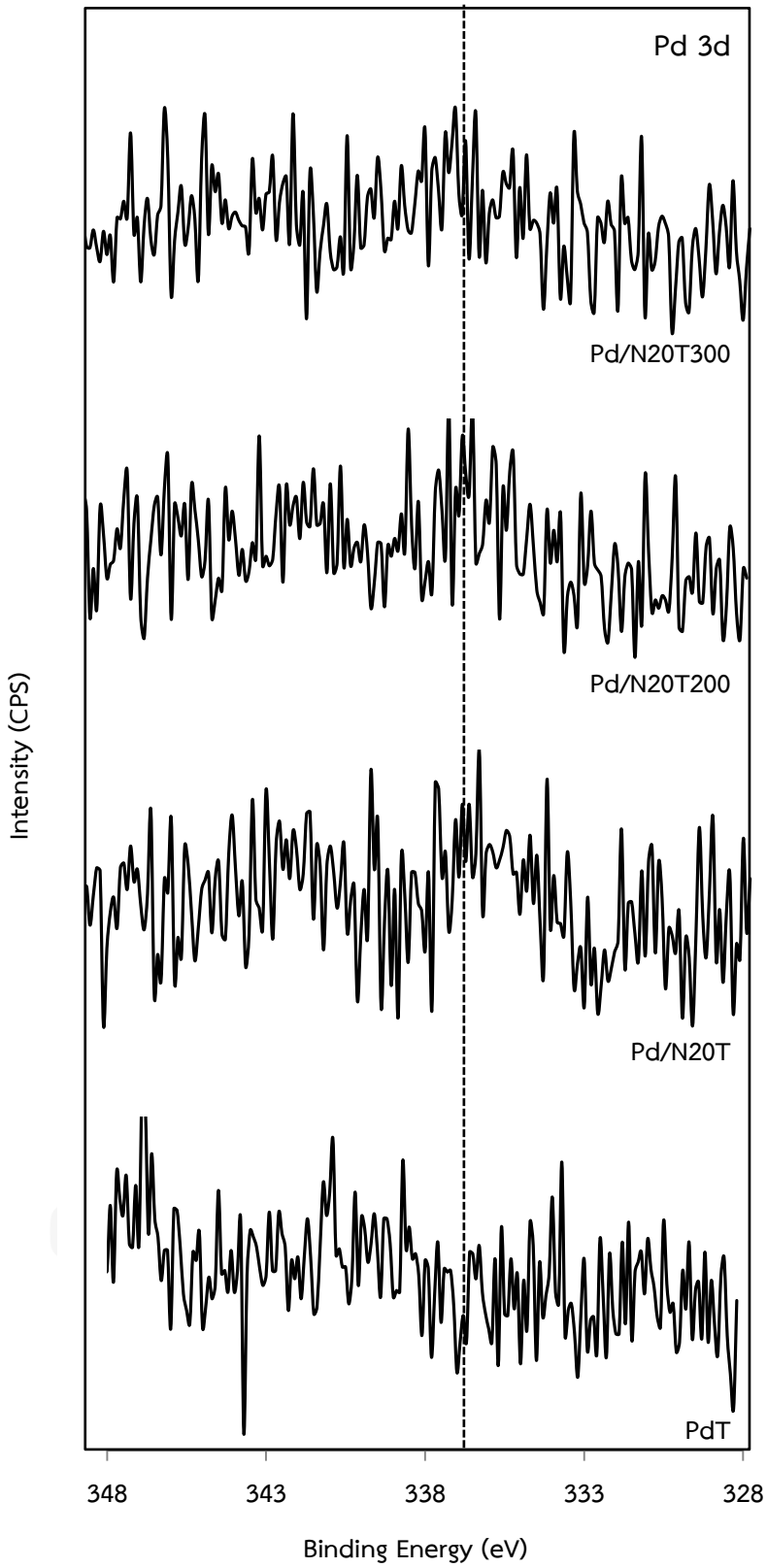

Figure 4.4 XPS Pd 3d core level of the all catalysts

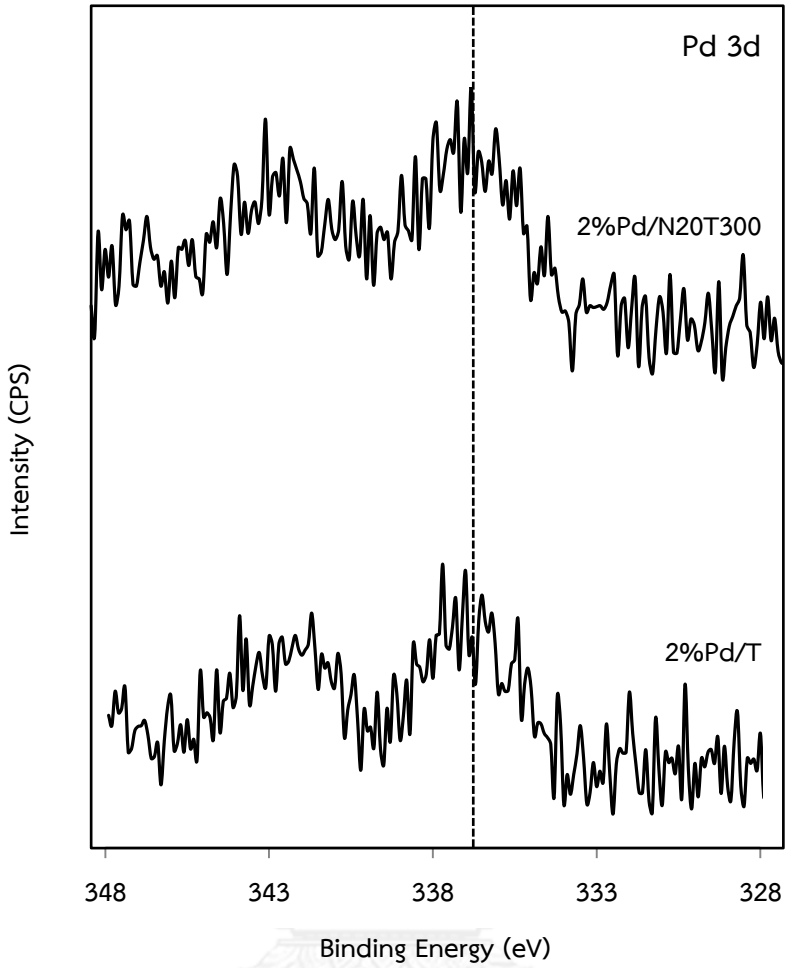

Figure 4.5 XPS Pd 3d core level of 2%Pd/T and 2%Pd/N20T300 catalysts

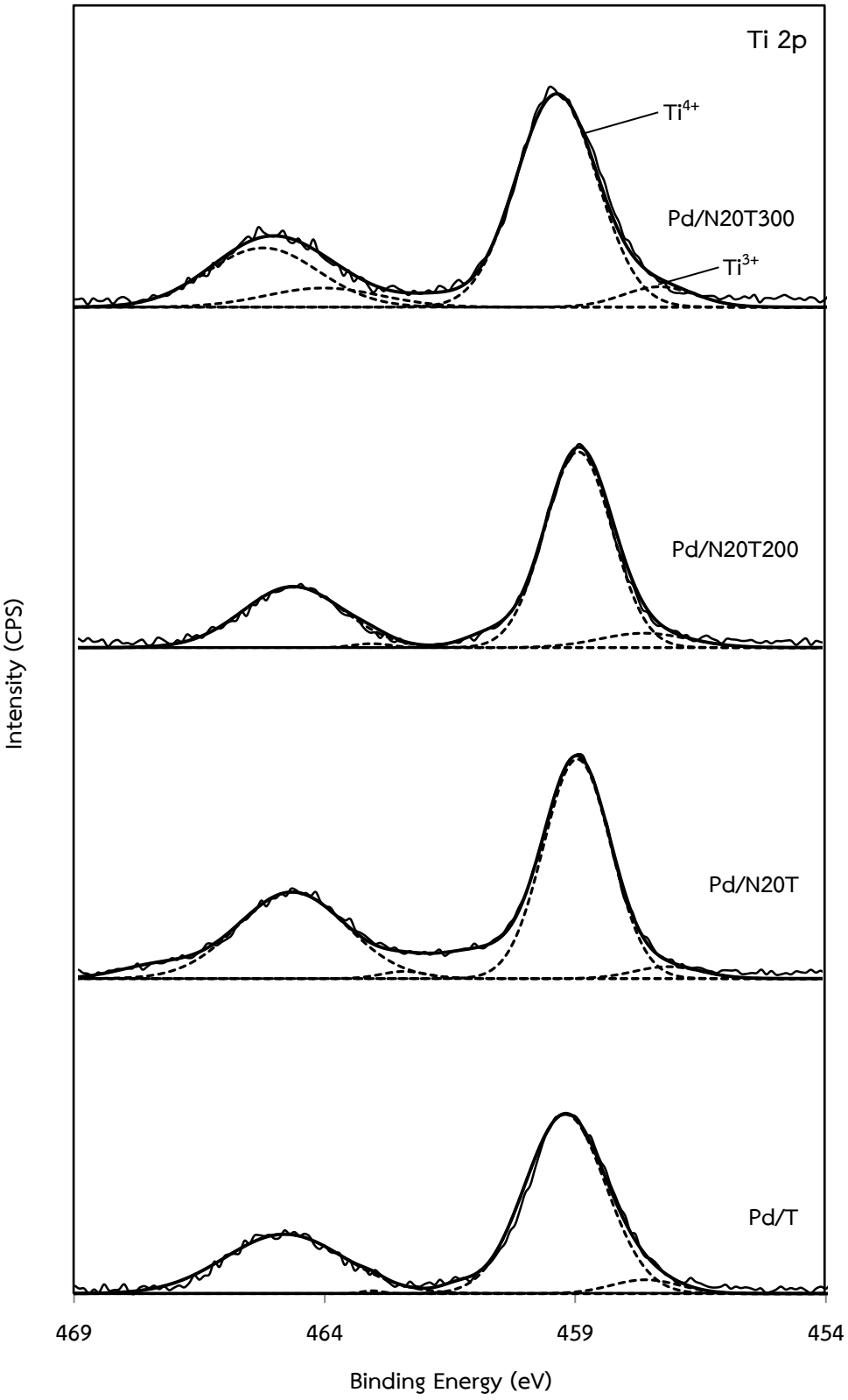

Figure 4.6 XPS Ti 2p spectra of the all catalysts

Figure 4.6 shows the Ti 2p XPS spectra for Pd/TiO_2 and Pd/N-doped TiO_2 with different calcination temperature. The experimental data points could be fitted by only two doublets, representing signals from Ti^{4+} and Ti^{3+} within the detection range of XPS. The presence Ti $2p_{3/2}$ peaks has a binding energies around 458.9-459.3 eV represents Ti^{4+} and Ti $2p_{3/2}$ peaks at low binding energies around 457.1-457.8 eV, which indicates that Ti^{3+} [64] and summarized in **Table 4.3.**

Table 4.3 The XPS Ti $2p_{3/2}$ of the all catalysts

Sample	Ti $2p_{3/2}$				
	Ti^{4+}		Ti^{3+}		% Ti^{3+}
	B.E. (eV)	Area	B.E. (eV)	Area	
Pd/T	459.2	6482.73	457.6	421.38	6.10
Pd/N20T	458.9	9356.91	457.1	507.67	5.14
Pd/N20T200	458.9	8846.16	457.6	803.02	8.78
Pd/N20T300	459.3	7053.42	457.3	603.14	7.88

Modification due to nitrogen atom substitution of oxygen atom in the TiO_2 lattice can result in lower B.E. of Ti 2p due probably to the covalence between Ti and N bond [65]. However, there was no clear indication of N-substituted O atom in the present work. Oxygen 1s core level was also detected at 530.2-530.6 eV, which can be referred to O^{2-} ion in the TiO_2 lattice [66].

4.1.1.4 UV-visible spectrophotometer (UV-vis)

The presence of nitrogen in the TiO_2 structure was confirmed by the UV-visible spectroscopy. The UV-visible light absorption spectra of the T, N20T, N20T200 and N20T300 supports are shown in the **Figure 4.7.**

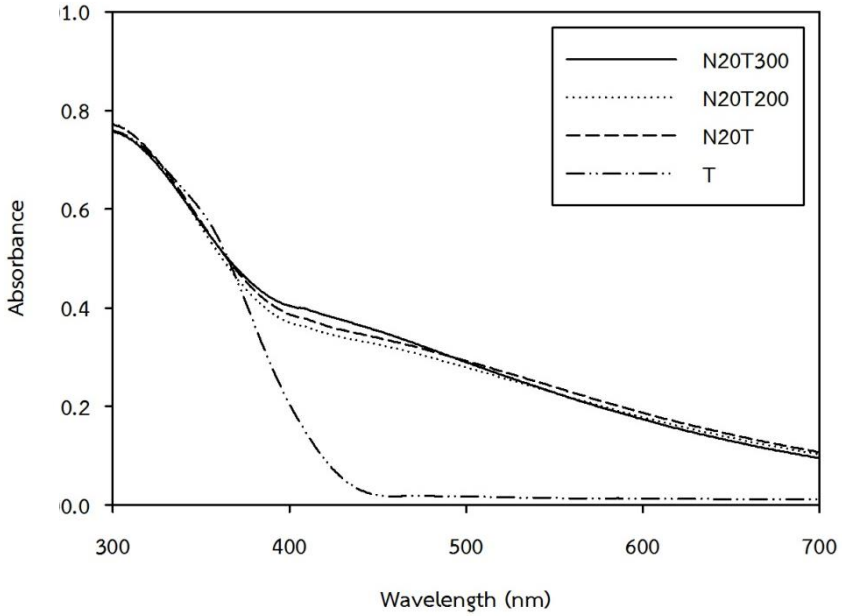

Figure 4.7 UV-visible light absorption spectra of the T, N20T, N20T200 and 20T300 supports

It was found that the addition of nitrogen with different calcination temperatures resulted in broad and descending absorption spectra in the wavelength range of 390 to 700 nm compared to the bare TiO_2 support which the adsorption edge appeared at wavelength 420 nm.

An increase in visible light adsorption also corresponded to the yellow brown color of the nitrogen doped TiO_2 supports. The calcination temperature used for calcinations of N-doped TiO_2 supports had little effect in the absorption in the wave in the visible light region.

4.1.1.5 Fourier transform infrared spectroscopy (FT-IR)

The FT-IR spectra were carried out in wavenumbers 500-4000 cm^{-1} in order to determine presence the functional groups and the results are shown in **Figure 4.8, Figure 4.9** and **Figure 4.10,** respectively.

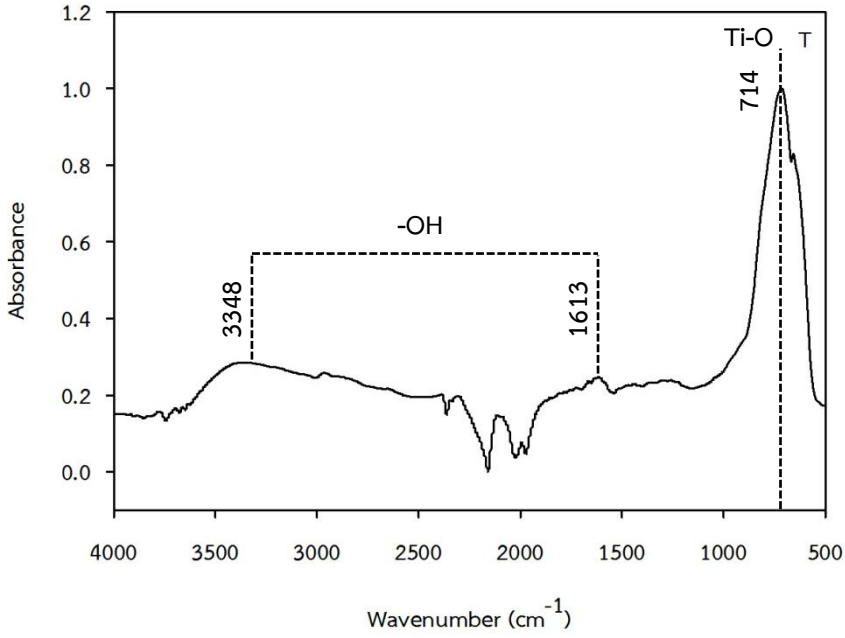

Figure 4.8 FT-IR spectra of the TiO_2 support

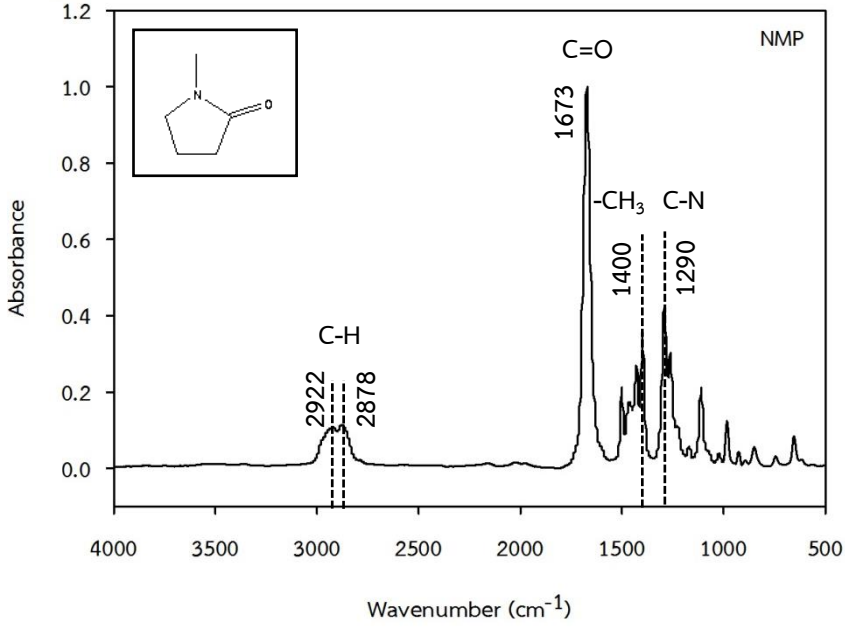

Figure 4.9 FT-IR spectra of the NMP solution

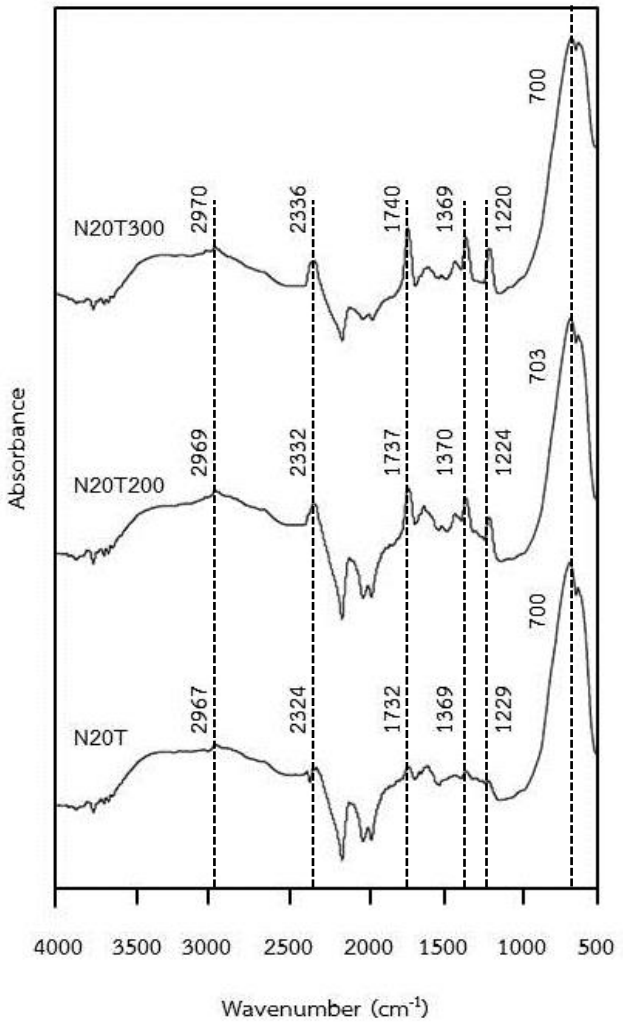

Figure 4.10 FT-IR spectra of the N20T, N20T200 and N20T300 supports

Figure 4.8 shows the FT-IR spectra of the TiO_2 support The OH of water of crystallization was absorbed in the region 1600-1630 cm^{-1} for the lattice hydroxyl and the OH of water of crystallization was absorbed in the region 3100-3600 cm^{-1} for surface hydroxyl. The Ti-O stretching vibration has been found in the range 660-750 cm^{-1} [67].

For the FT-IR spectra of the NMP solution as shown in **Figure 4.9,** the C-H stretching vibration occurred in the region 2840-2975 cm^{-1} and the $-CH_3$ symmetric bending vibration occurred in the region 1350-1410 cm^{-1}. The carbonyl group, the C=O absorbed strong intensity at intense peak around 1670-1820 cm^{-1}. For the C-N have an absorption band of medium intensity in the range 1080-1360 cm^{-1}.

Figure 4.10 shows that the OH groups on the lattice hydroxyl and surface hydroxyl appeared broad band around wavenumbers 3350 cm^{-1} and 1610 cm^{-1}, respectively. For all support, the Ti-O band shown highly intense peak around wavenumbers 700-703 cm^{-1}. These results indicate that the intensity peak of the C-H stretching, the $-CH_3$ symmetric bending, the C=O and the C-N increased in with increasing calcination temperature used. In addition, found that absorption of peak at around 2324-2336 cm^{-1} may be due to the C-H stretching vibration [68].

4.1.1.6 Transmission electron microscopy (TEM)

The TEM images and Pd particle size distribution of the Pd/T catalyst and the Pd/N20T300 catalyst are presented in **Figure 4.11, 4.12, 4.13** and **4.14,** respectively. The morphology of the Pd/T catalyst and the Pd/N20T300 catalyst were observed as spherical particles. Pd particles catalyst supported on both the N-doped TiO_2 support and the TiO_2 support were highly dispersed.

The Pd particles on catalyst supported nitrogen doped TiO_2 support calcined at 300°C were slightly decreased 1.5 nm to 1.0 nm, compared to the TiO_2 support.

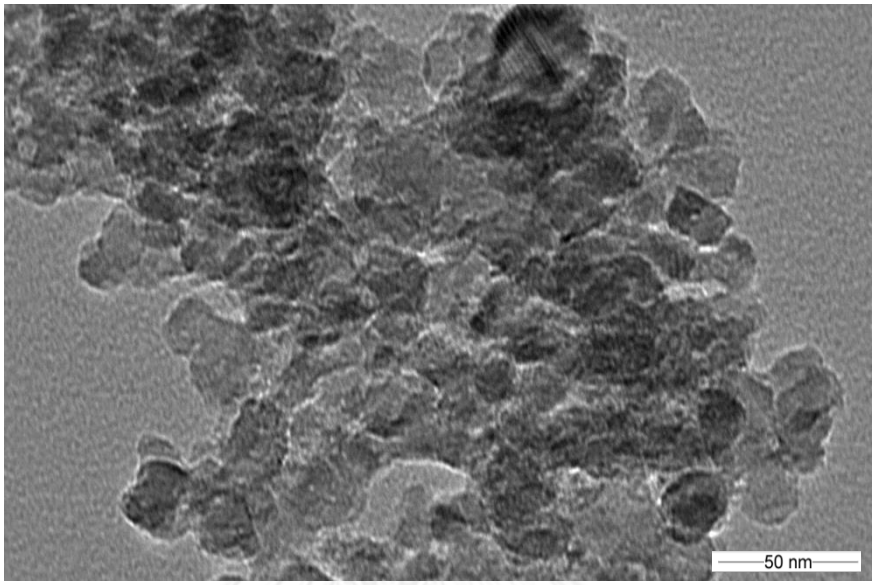

Figure 4.11 TEM images of the Pd/T catalyst

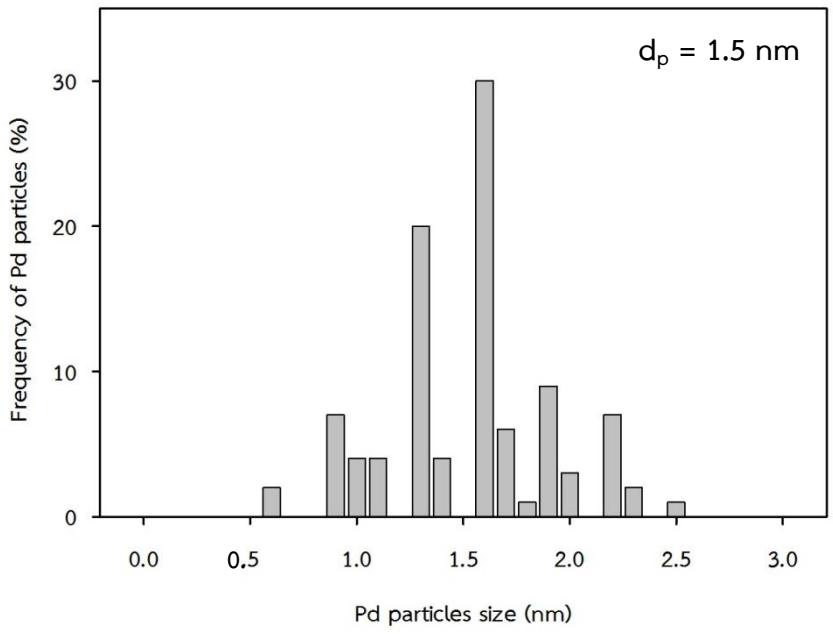

Figure 4.12 Pd particles size distribution of the Pd/T catalyst

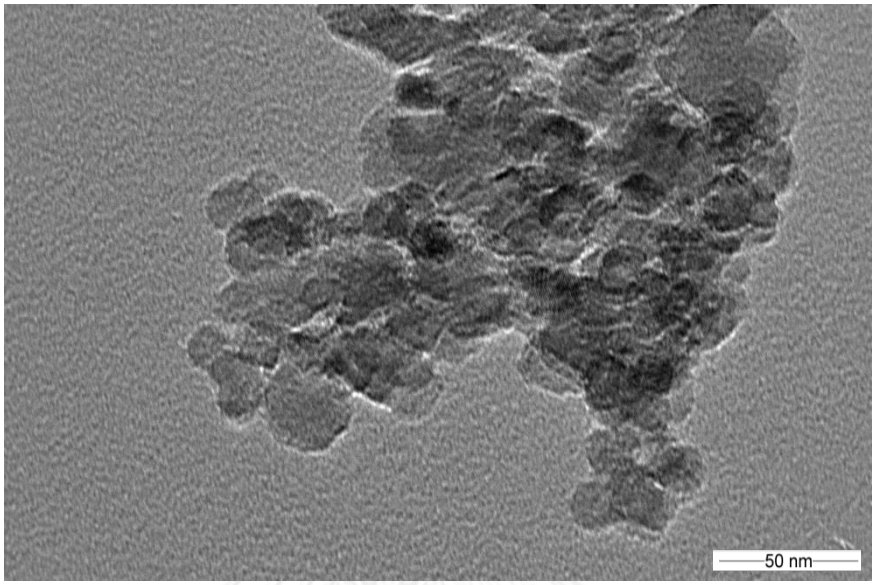

Figure 4.13 TEM images of the Pd/N20T300 catalyst

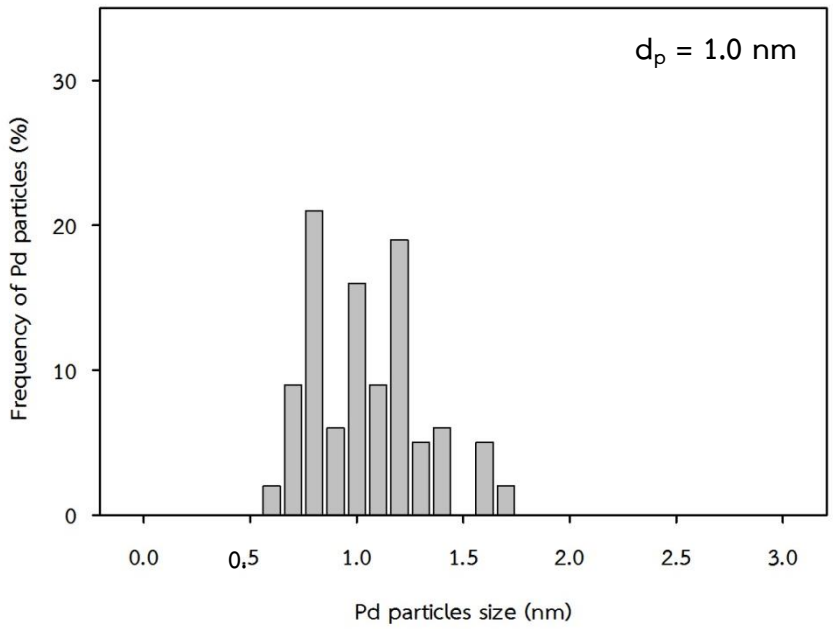

Figure 4.14 Pd particles size distribution of the Pd/N20T300 catalyst

4.1.1.7 H_2 chemisorption

The amounts of H_2 chemisorption of all the catalysts are given in **Table 4.4,** which related to amount of active surface Pd metal on the catalysts, %Pd dispersion and average Pd^{o} particle size. The %Pd dispersion was determine by the stoichiometric factor H/Pd = 1 [69] and the average Pd^{o} particle size was calculated base on : d_p Pd^{o} (nm) = 1.1/D, where D is the fractional metal dispersion [70].

For the nitrogen doping on TiO_2 supports with different calcination temperatures, the amounts of H_2 consumption increased with increasing calcination temperature used from without the calcination to with the calcination in air at 200°C, the Pd active site increased from 2.95×10^{18}-5.19×10^{18} H_2 molecule/g-catalyst, Pd dispersion increased from 10.44-18.34% and average Pd^{o} particle size decreased from 10.53-6.00 nm. However, the amount of H_2 consumption slightly decreased when the calcination temperature increased to 300°C, the Pd active site was 3.22×10^{18} H_2 molecule/g-catalyst and Pd dispersion was 11.39% and average Pd^{o} particle size was 9.66 nm. The results suggested that the nitrogen doping with the constant amount of NMP solution at different calcination temperatures affected the amounts of H_2 consumption of all the catalysts. All the Pd catalysts supported on N-doped TiO_2 supports consumed higher amounts hydrogen than the Pd catalysts supported on TiO_2 support.

Table 4.4 The amounts of H_2 consumption of all the catalysts

Sample	H_2 consumption (μL/g-catalyst)	Pd active sites ($\times10^{-18}$ molecule/g-catalyst)	Pd dispersion (%)	d_p Pd^{o} (nm)
Pd/T	40.72	2.19	7.7	14.2
Pd/N20T	54.97	2.95	10.4	10.6
Pd/N20T200	96.56	5.19	18.3	6.0
Pd/N20T300	60.00	3.22	11.3	9.7

The calculated particles size were much larger than those base on TEM analysis. However, the Pd particles catalyst supported on TiO_2 support were larger than the Pd particles catalyst supported on N20T300 support which were similar trend as those in **Figure 4.12** and **Figure 4.14.**

4.1.2 Catalytic activity

The catalytic activity of the Pd catalysts supported on N-doped TiO_2 supports with different calcination temperatures and TiO_2 support were evaluated in the liquid phase selective hydrogenation of 1-heptyne. The products of 1-heptene hydrogenation reaction which were detected by a CG after termination of the reaction testing were 1-heptyne (desired product) and n-heptane.

The conversion of 1-heptyne and the selectivity to 1-heptene as a function of time on stream over the Pd/T, Pd/N20T, Pd/N20T200 and Pd/N20T300 catalysts are shown in **Figure 4.15** and **Figure 4.16.** All the Pd catalysts supported on N-doped TiO_2 supports exhibited higher activity than Pd catalysts supported on TiO_2 support. The hydrogenation rate was in the order Pd/N20T = Pd/N20T200 = Pd/N20T300 > Pd/T which the hydrogenation of 1-heptyne was complete in 60 min for all the Pd catalysts supported on N-doped TiO_2 supports and 120 min for Pd catalysts supported on TiO_2 support. The hydrogenation activity corresponded to the amounts Pd active sites, %Pd dispersion and average Pd° particle size as reported in **Table 4.4.** The Pd/N20T300 catalyst with higher activity showed higher dispersion and smaller average Pd particles size. However, the selectivity of heptene at final reaction time was found to be in the order Pd/N20T300 (90.1%) > Pd/T (86.8%) > Pd/N20T200 (80.4%) > Pd/N20T (71.5%).

Nitrogen doping on titania affected the formation of Ti^{3+} [59, 71]. It is expected that the nitrogen atoms substitution oxygen atoms in the TiO_2, this imply that the N atoms could incorporated with Ti [65].

The Pd/N20T catalyst showed 5.14% of Ti^{3+} (data from Table 4.3) due to the surface area of titania partially covered from solvent, it may be eclipsed as Ti^{3+} occurring has small amounts. As a result, the selectivity of heptene which is less as well. When with calcination temperature at 200°C, the Pd/N20T200 catalyst

presented the highest Ti^{3+} as 8.87%. However, the selectivity of heptane is not the highest because the nitrogen atom may be blocked contention between Pd and Ti^{3+} and when increasing the calcination temperature at 300°C, the Pd/N20T300 catalyst presented of Ti^{3+} as 7.88%. Reducing the amount of Ti^{3+} as a result of the dislodgement of partially nitrogen atoms. So, the opportunity Pd can be contact with Ti^{3+} on surface TiO_2 has increased, effect on strong interaction between Pd with TiO_2 support resulting in higher selectivity of heptene.

The yield of heptene product and the performance plots of 1-heptyne hydrogenation on the Pd/T, Pd/N20T, Pd/N20T200 and Pd/N20T300 catalysts are shown in **Figure 4.17** and **Figure 4.18.** The yield of heptane product was found to be in the order Pd/N20T300 (94.1%) at 60 min > Pd/N20T (91.7%) at 60 min > Pd/T (86.84%) at 120 min > Pd/N20T200 (86.0%) at 60 min. The Pd/N20T300 catalyst exhibited the best performance of 1-heptyne hydrogenation (~90% heptane selectivity) at complete conversion of 1-heptyne.

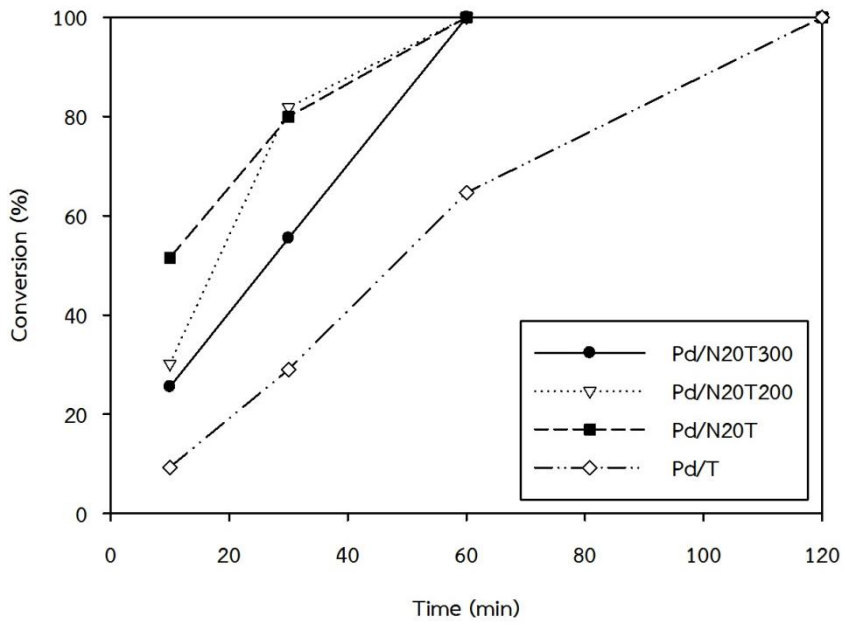

Figure 4.15 Hydrogenation of 1-heptyne on the Pd/T, Pd/N20T, Pd/N20T200 and Pd/N20T300 catalysts

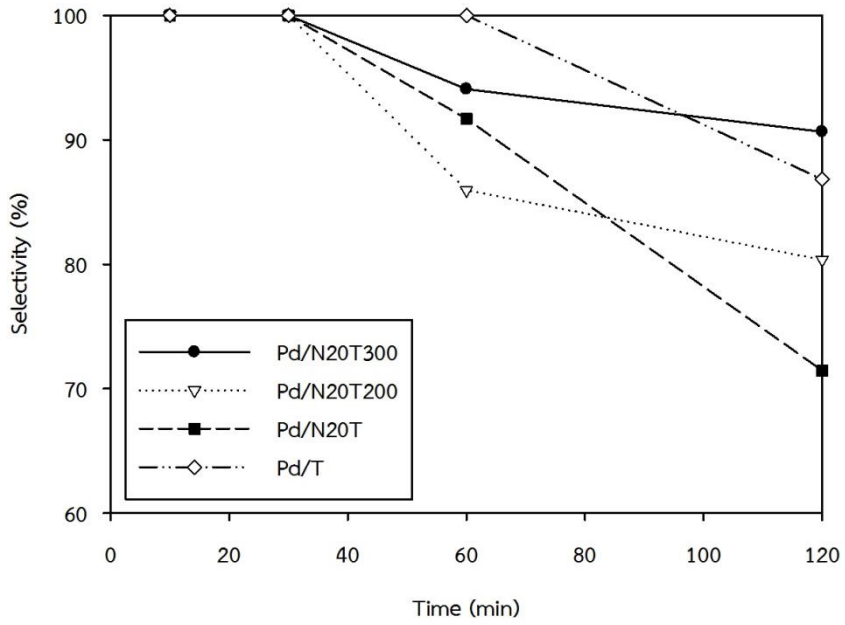

Figure 4.16 Heptene selectivity in hydrogenation of 1-heptyne on the Pd/T, Pd/N20T, Pd/N20T200 and Pd/N20T300 catalysts

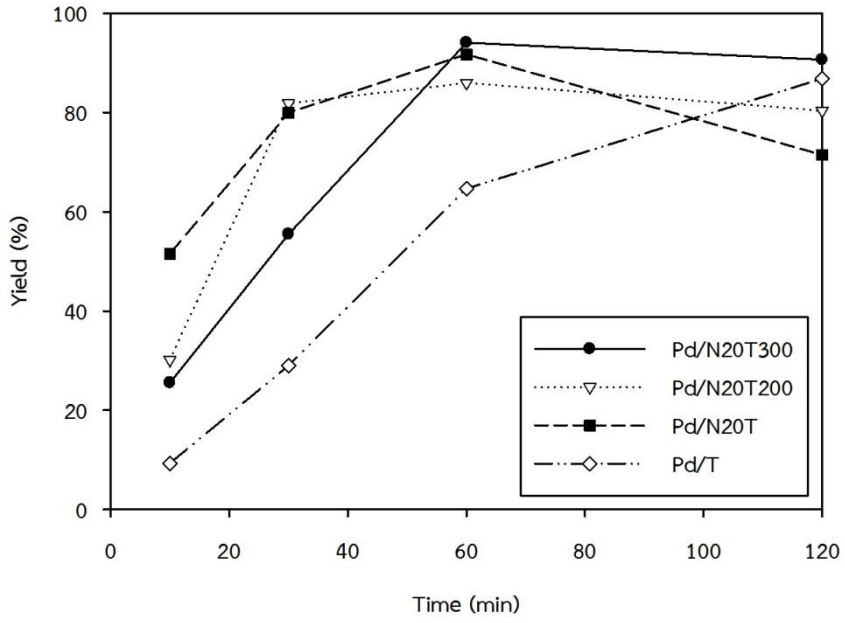

Figure 4.17 Yield of heptene product on the Pd/T, Pd/N20T, Pd/N20T200 and Pd/N20T300 catalysts

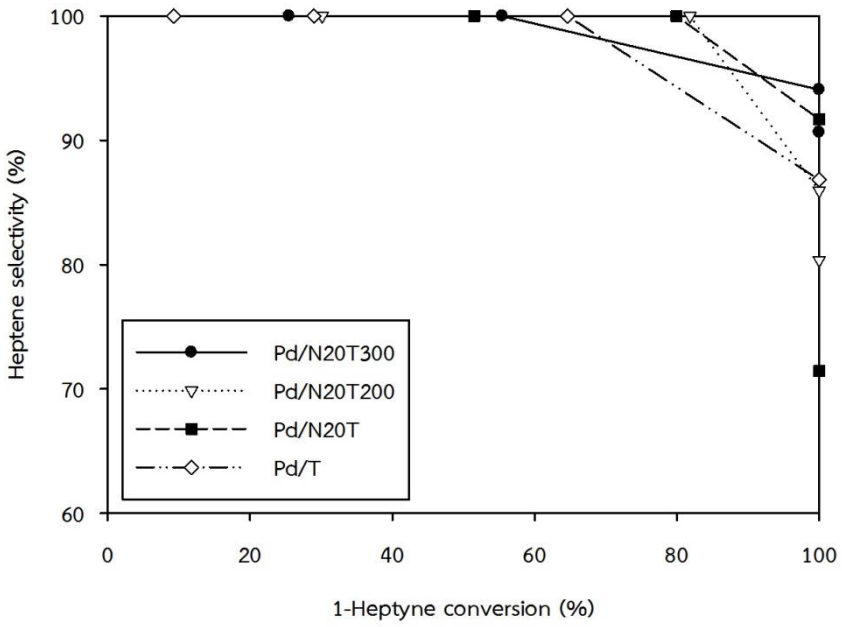

Figure 4.18 The performance of 1-heptyne hydrogenation over the Pd/T, Pd/N20T, Pd/N20T200 and Pd/N20T300 catalysts

4.2 The effect of the amounts nitrogen doping on TiO_2 supports

In this section, the catalyst suitable for the reaction study in previously section was selected. Among the catalysts in this study, the Pd catalyst supported on N-doped TiO_2 supports calcined in air at 300°C for 2 h exhibited the best catalytic performance, in which relatively high heptane selectivity (~90%) was obtained at complete conversion of 1-heptyne.

N-doped TiO_2 supports with various amounts of nitrogen doping on TiO_2 support were synthesized and calcined in air at 300°C for 2 h. The TiO_2 supports were prepared by the sol-gel method using the same conditions in the previously section. The N-doped TiO_2 supports were synthesized by using NMP solution as a nitrogen source with different amounts of NMP solution (10, 15, 20, 30 and 50 ml, respectively). The NMP solution was added to 2 g of TiO_2 supports with mixed continuously and heated at 170°C for 4 h then dried in air overnight at 110°C followed by calcination in air at 300°C for 2 h. N-doped TiO_2 supports were labeled as N10T300, N15T300, N20T300, N30T300 and N50T300, respectively. All the catalysts

were prepared by wet impregnation method using $PdCl_2$ as a Pd precursor with loading 0.5%wt Pd and calcined in air flow at 450°C for 3 h to eliminate chloride contamination and the catalysts were labeled as Pd/N10T300, Pd/N15T300, Pd/N20T300, Pd/N30T300 and Pd/N50T300, respectively.

4.2.1 Catalysts characterization

4.2.1.1 X-ray diffraction (XRD)

Phase identification of the supports and the catalysts were based on the results from x-ray diffraction analysis. The XRD patterns of the N-doped TiO_2 supports with different amounts of NMP solution and calcination temperature at 300°C are shown in **Figure 4.19.** The XRD patterns for all the supports exhibited XRD characteristic peaks at 26° (the major of anatase phase), 36°, 48°, 56°, 63°, 69° and 75° 2 theta with small amounts of rutile phase appeared at 28°, 36° and 41° 2 theta and brookite phase at 31° 2 theta. The rutile phase content increased in the order N20T300 > N15T300 = N30T300 > N10T300 > N50T300.

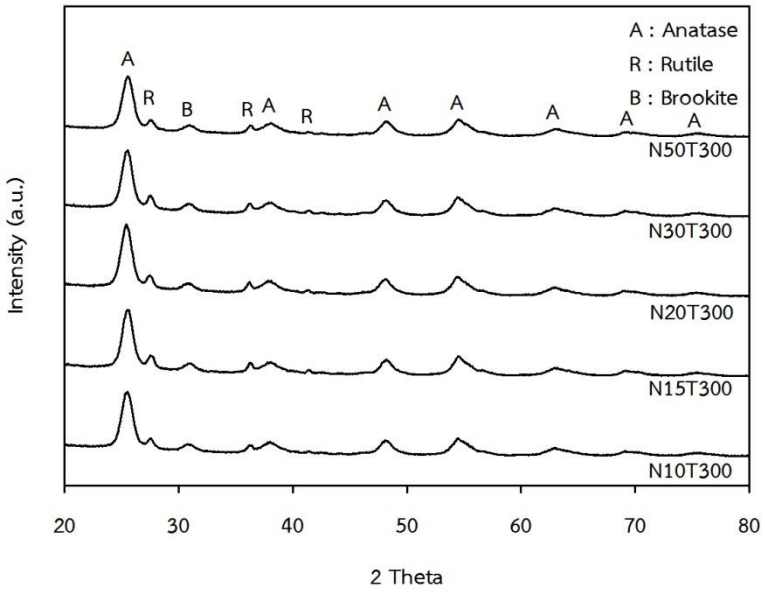

Figure 4.19 XRD patterns of the N-doped TiO_2 supports with different amounts of NMP solution and calcination temperature at 300°C

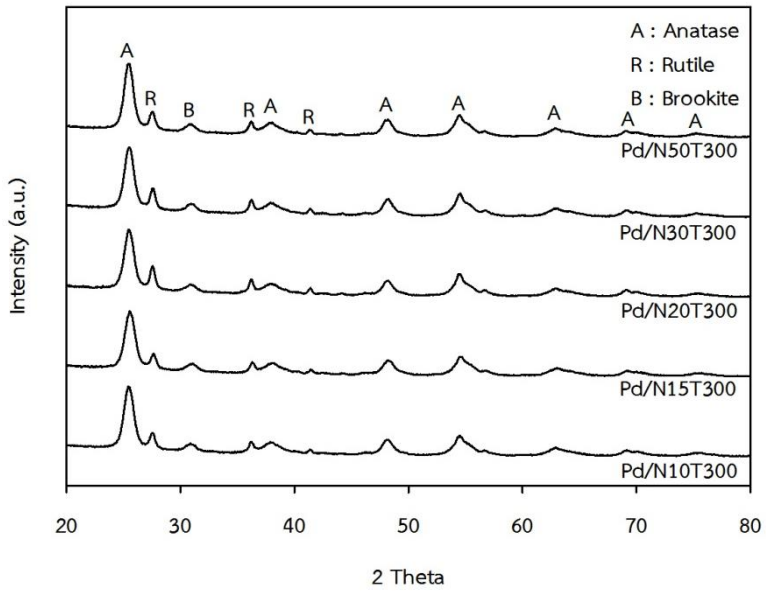

Figure 4.20 XRD patterns of the Pd catalysts supported on N-doped TiO_2 supports with different amounts of NMP solution and calcination temperature at 300°C

However, the XRD characteristic peaks of the Pd catalysts supported on N-doped TiO_2 supports with different amounts of NMP solution and calcination temperature at 300°C are shown in **Figure 4.20.** The XRD patterns for all the catalysts exhibited XRD characteristic peaks that appeared at 26° (the major of anatase phase), 36°, 48°, 56°, 63°, 69° and 75° 2 theta with small amounts of rutile phase appeared at 28°, 36° and 41° 2 theta and brookite phase at 31° 2 theta same as in **Figure 4.19.**

For all the catalysts, the major anatase phase and the rutile phase content increased in the order Pd/N10T300 > Pd/N15T300 > Pd/N20T300 > Pd/N30T300 > Pd/N50T300 and the peaks corresponding to the formation of PdO were not detected due to low loading Pd content and high dispersion of the Pd catalysts supported on N-doped TiO_2 supports and TiO_2 support as presented in **Table 4.5** and corresponding to TEM micrographs in **Figure 4.26** and **Figure 4.28.**

4.2.1.2 N_2 physisorption

The BET surface area, pore volume, average pore size and hyteresis loop of all the catalysts were measured by N_2 physisorption technique. The results are given in **Table 4.5.** The BET surface of the Pd catalyst supported on N-doped TiO_2 supports with different amounts of NMP solution and calcination temperature at 300°C decreased in with increasing amounts of added NMP solution [70] from 106.3-95.5 m^2/g because the Pd catalysts supported on N-doped TiO_2 supports were agglomerated during increasing amounts of NMP solution or surface area of TiO_2 coated with excess NMP solution. Similar finding were also previous researches [72, 73]. Pore volume of all the catalysts was not much different, which was approximately 0.2-0.3 cm^3/g.

The hyteresis loop of nitrogen adsorption-desorption isotherms consists of adsorption region and desorption region that hyteresis loop can be used to predict pore characteristics of materials. The nitrogen adsorption-desorption isotherms at -196°C of the Pd catalysts supported on N-doped TiO_2 supports with different amounts of NMP solution and calcination temperature at 300°C are shown in **Figure 4.21.**

Table 4.5 Physical properties of the Pd catalysts supported on N-doped TiO_2 supports with different amounts of NMP solution and calcination temperature at 300°C

Sample	BET surface area (m^2/g)	Pore volume (cm^3/g)	Average pore size (nm)
Pd/N10T300	106.3	0.26	6.1
Pd/N15T300	104.7	0.21	5.0
Pd/N20T300	98.8	0.21	5.3
Pd/N30T300	97.6	0.21	5.0
Pd/N50T300	95.2	0.27	10.5

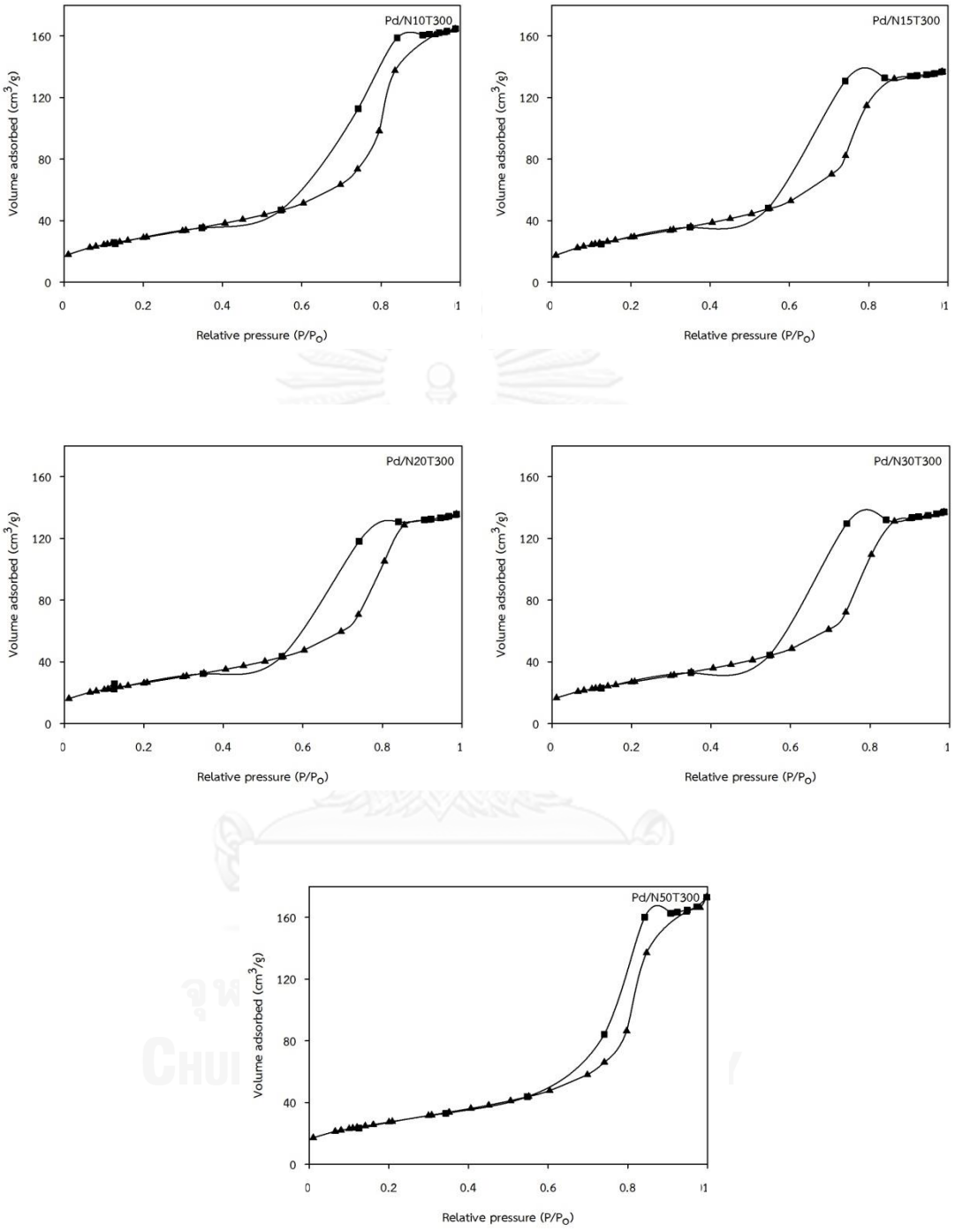

Figure 4.21 N_2 adsorption-desorption isotherms at -196°C of the Pd catalysts supported on N-doped TiO_2 supports with different amounts of NMP solution and calcination temperature at 300°C

These isotherms represent to the same hyteresis loop, with the typical mesoporous structure having pore size diameter ranging from 2-50 nm (IUPAC 1985 classification) [62] corresponding to data in **Table 4.5,** with average pore size around 5.0-10.5 nm.

4.2.1.3 X-ray photoelectron spectroscopy (XPS)

The XPS analysis including XPS spectra, binding energy, full width at half maximum (FWHM) and composition of the Pd catalysts on the surface layer of all the catalysts which reported in **Figure 4.22** and analysis results are summarized in **Table 4.6.**

The XPS spectra of the Pd 3d for all the catalysts are shown in **Figure 4.22**. The binding energy of Pd $3d_{5/2}$ for all the catalysts were seen at binding energies around 336.5-337.6 eV. Palladium was suggested to be in the PdO form [63].

The XPS peaks of N 1s for all the catalysts were not observed distinctively on the Pd/N10T300, Pd/N15T300, Pd/N20T300, Pd/N30T300 and Pd/N50T300 catalysts.

Table 4.6 The XPS of all the catalysts

Sample	Pd 3d		
	B.E. (eV)	FWHM (eV)	Atomic concentration (%)
Pd/N10T300	337.3	1.127	0.05
Pd/N15T300	337.6	0.602	0.04
Pd/N20T300	336.8	0.656	0.04
Pd/N30T300	336.5	0.505	0.02
Pd/N50T300	336.2	0.876	0.03

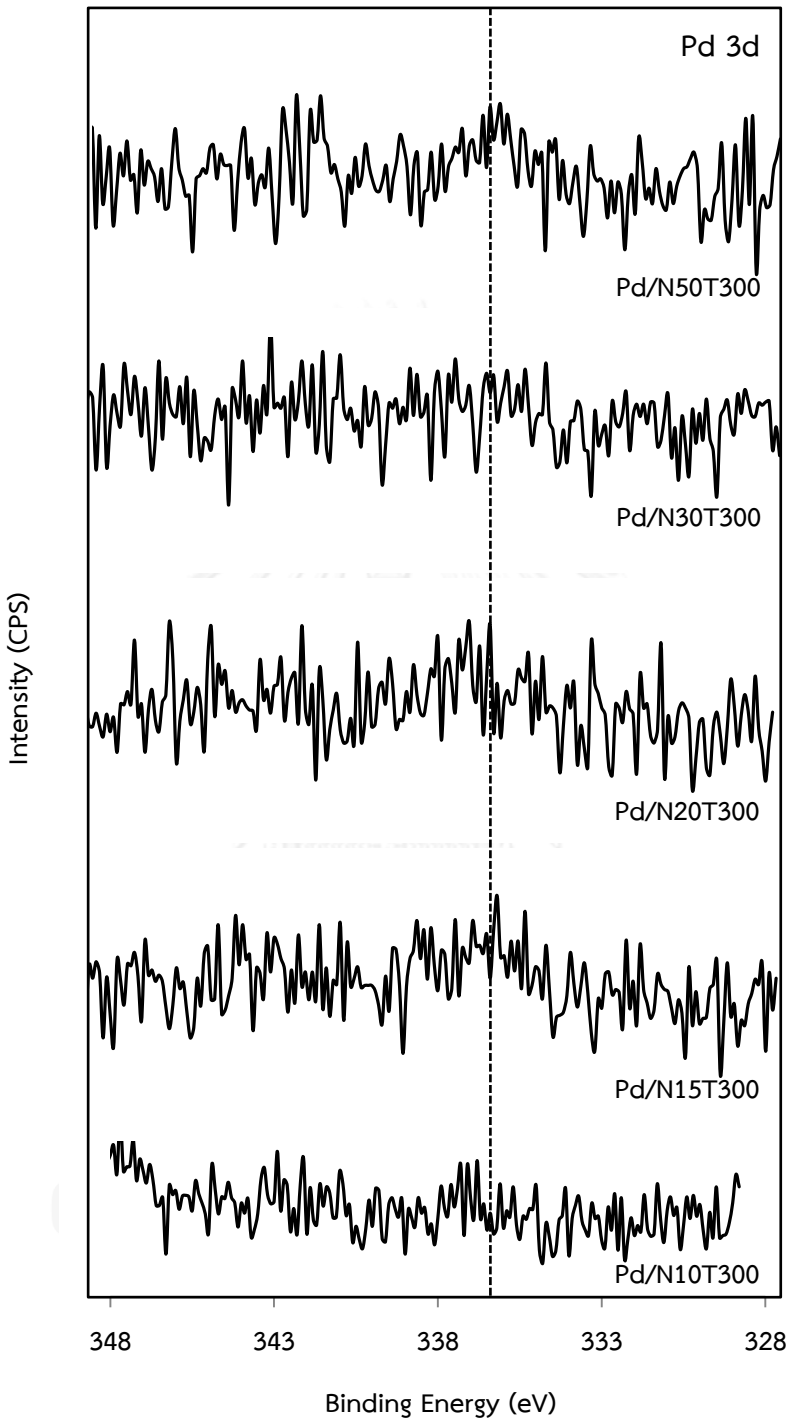

Figure 4.22 XPS Pd 3d core level of the Pd/N10T300, Pd/N15T300, Pd/N20T300, Pd/N30T300 and Pd/N50T300 catalysts

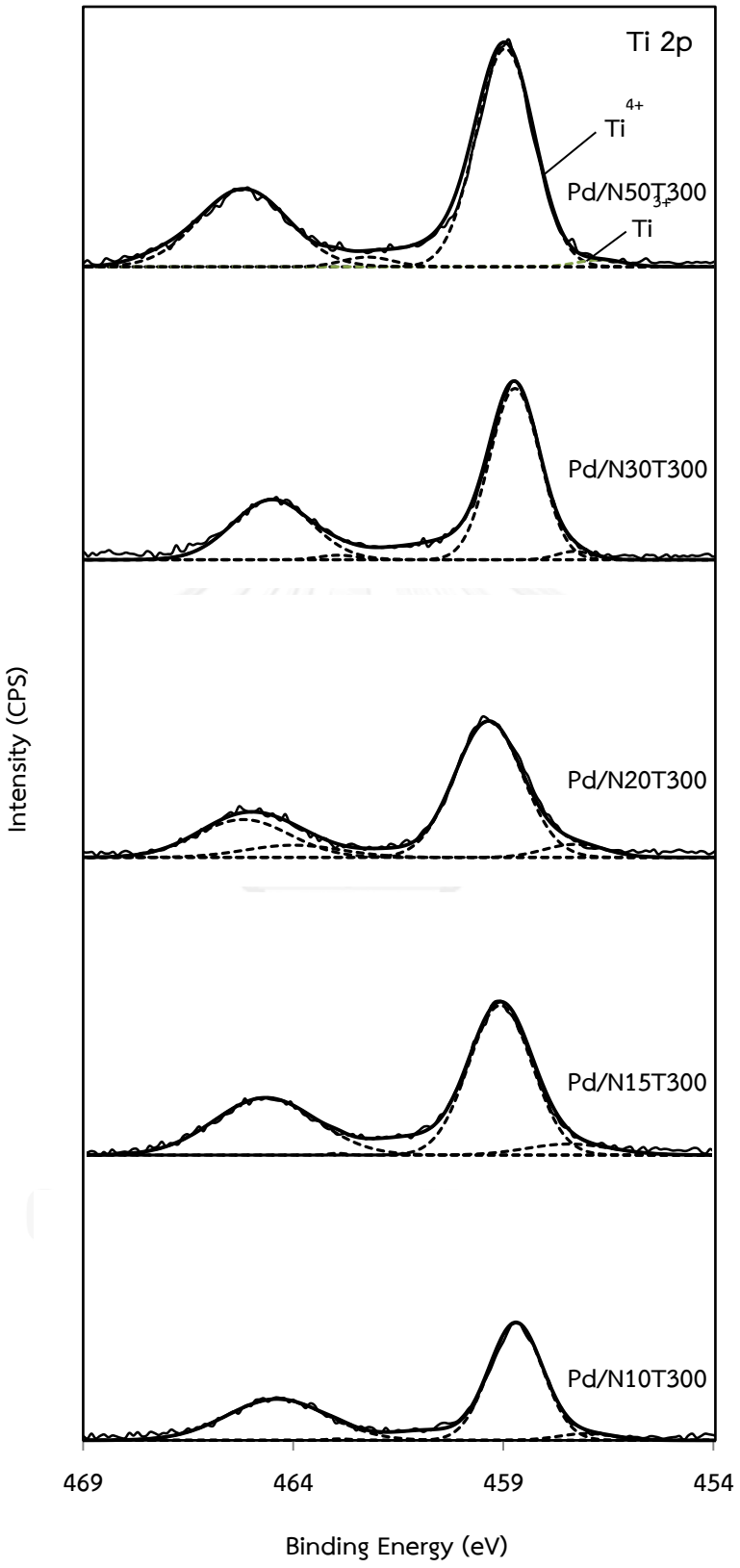

Figure 4.23 XPS Ti 2p spectra of the all catalysts

Table 4.7 The XPS Ti $2p_{3/2}$ of the all catalysts

Sample	Ti $2p_{3/2}$				
	Ti^{4+}		Ti^{3+}		% Ti^{3+}
	B.E. (eV)	Area	B.E. (eV)	Area	
Pd/N10T300	458.7	4227.50	457.0	260.45	5.80
Pd/N15T300	459.1	7367.84	457.4	720.25	8.91
Pd/N20T300	459.3	7053.42	457.3	603.14	7.88
Pd/N30T300	458.7	6708.25	457.3	228.01	3.29
Pd/N50T300	459.2	8964.59	457.7	222.89	2.43

Modification due to nitrogen atom substitution of oxygen atom in the TiO_2 lattice can result in lower B.E. of Ti 2p due probably to the covalence between Ti and N bond [65]. **Figure 4.23** shows the Pd catalysts supported on N-doped TiO_2 supports with different amounts of NMP solution and calcination temperature at 300°C. A small amount of NMP solution added to the TiO_2 supports. This decrease chances of corporation between Ti and N and increasing amounts of added NMP solution change to increase of corporation between Ti and N. However, the excess NMP solution results in reducing the presence of Ti^{3+} because some of TiO_2 surface were covered with NMP solution or agglomerated during increasing amounts of NMP solution [72, 73] and analysis results are summarized in **Table 4.7.**

However, there was no clear indication of N-substituted O atom in the present work. Oxygen 1s core level was also detected at 530.0-530.4 eV, which can be referred to O^{2-} ion in the TiO_2 lattice [66].

4.2.1.4 UV-visible Spectrophotometer (UV-vis)

The presence of nitrogen in the titania structure was confirmed by the UV-visible spectroscopy. The UV-visible light absorption spectra of the Pd/N10T300, Pd/N15T300, Pd/N20T300, Pd/N30T300 and Pd/N50T300 catalysts are

shown in the **Figure 4.24**. It was found the addition of nitrogen with different amounts of NMP solution and calcination temperature at 300°C resulted in broad and descending absorption spectra in the wavelength range of 390 to 700 nm compared to the bare titania support which the adsorption edge appeared at wavelength 420 nm. An increase in visible light adsorption also corresponded to the yellow brown color of the nitrogen doped titania supports. The amounts of added NMP solution for calcination of the nitrogen doped titania supports at 300°C had little effect in the absorption in the wave in the visible light region.

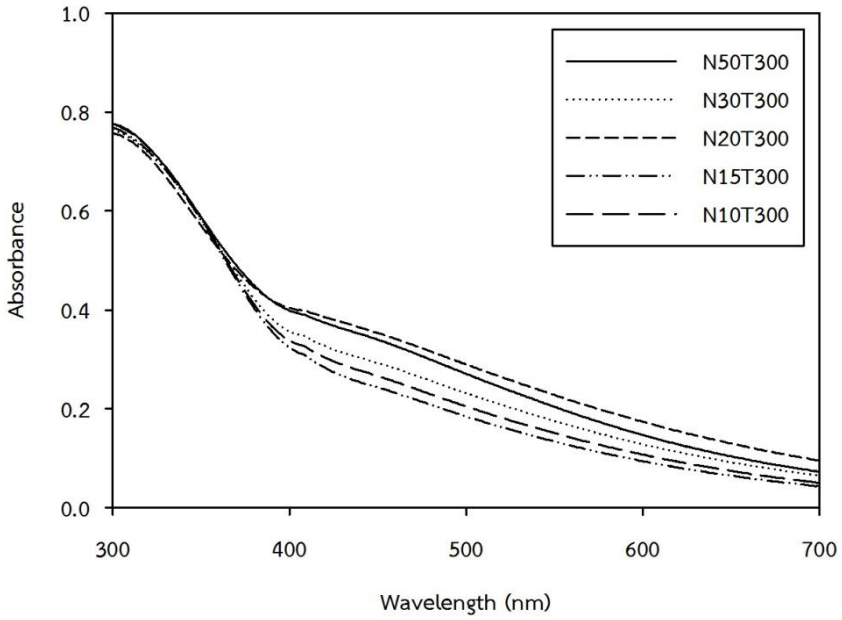

Figure 4.24 UV-visible light absorption spectra of the N10T300, N15T300, N20T300, N30T300 and N50T300 supports

4.2.1.5 Fourier transform infrared spectroscopy (FT-IR)

FT-IR spectra were carried out in wavenumbers 500-4000 cm^{-1} in order to determine the presences of functional groups are shown in **Figure 4.25.** The TiO_2 support, the OH of water of crystallization was absorbed in the region 1600-1630 cm^{-1} for the lattice hydroxyl and absorbed in the region 3100-3600 cm^{-1} for surface hydroxyl. Ti-O stretching vibration has been found in the range 660-750 cm^{-1} [67].

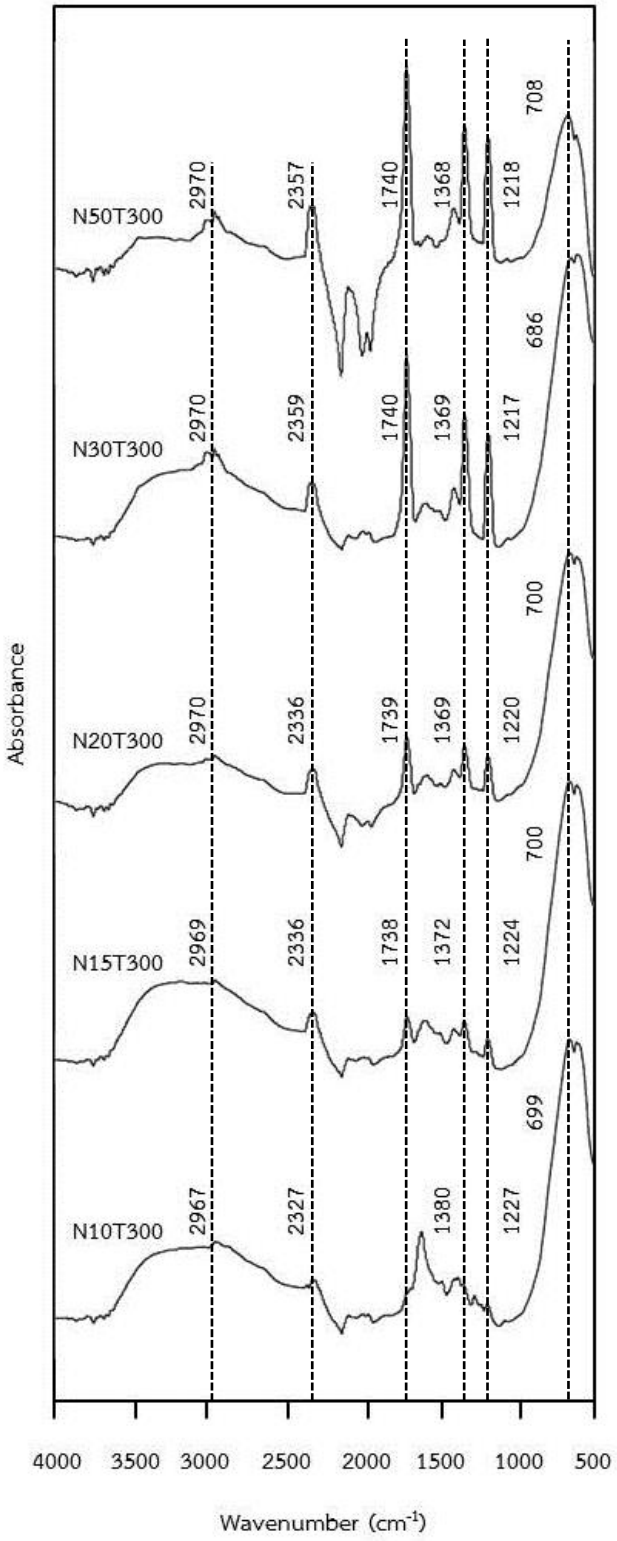

Figure 4.25 FT-IR spectra of the N-doped TiO_2 supports

Figure 4.25 shows the FT-IR spectra of the N-doped TiO_2 supports with different amounts of NMP solution and calcination temperature at 300°C. In this study, for all the N-doped TiO_2 supports appeared as broad band around wavenumbers 3350 cm^{-1} which indicated that the OH groups on the lattice hydroxyl and 1610 cm^{-1} indicated that the OH groups on the surface hydroxyl. The Ti-O band showed peaks around wavenumbers 686-708 cm^{-1}. The C-H stretching vibration occurred in the region 2964-2870 cm^{-1} and the $-CH^3$ symmetric bending vibration occurred in the region 1368-1380 cm^{-1}. The carbonyl group, the C=O absorbed strong intensity at intense peak around 1740-1738 cm^{-1}. For the C-N have an absorption band of medium intensity in the range 1218-1227 cm^{-1} and found that absorption of peak at around 2327-2357 cm^{-1} may be the C-H stretching vibration [68]. These patterns indicated that higher amounts of nitrogen doping led to increase in peak intensity.

4.2.1.6 Transmission electron microscopy (TEM)

The TEM images and Pd particle size distribution of Pd/N10T300 and Pd/N50T300 are presented in **Figure 4.26, 4.27, 4.28** and **4.29,** respectively. The morphology of the Pd/N10T300 catalyst and the Pd/N50T300 catalyst were observed as spherical shape particles and Pd particles were well dispersed on both supports.

However, increasing amounts of the NMP solution and calcination temperature at 300°C appeared to have similar Pd particle size on the Pd/N10T300 and the Pd/N50T300 catalysts in the range 0.8 nm to 1.0 nm.

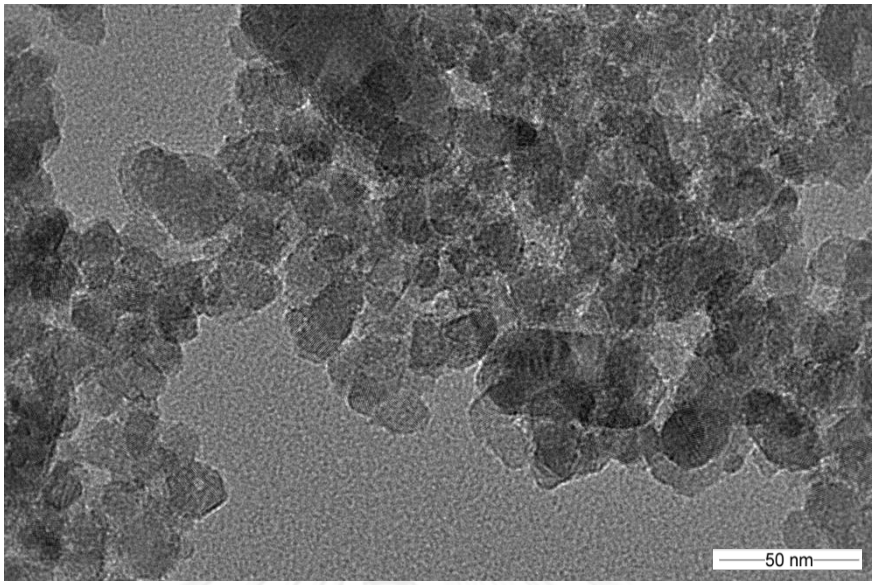

Figure 4.26 TEM images of the Pd/N10T300 catalyst

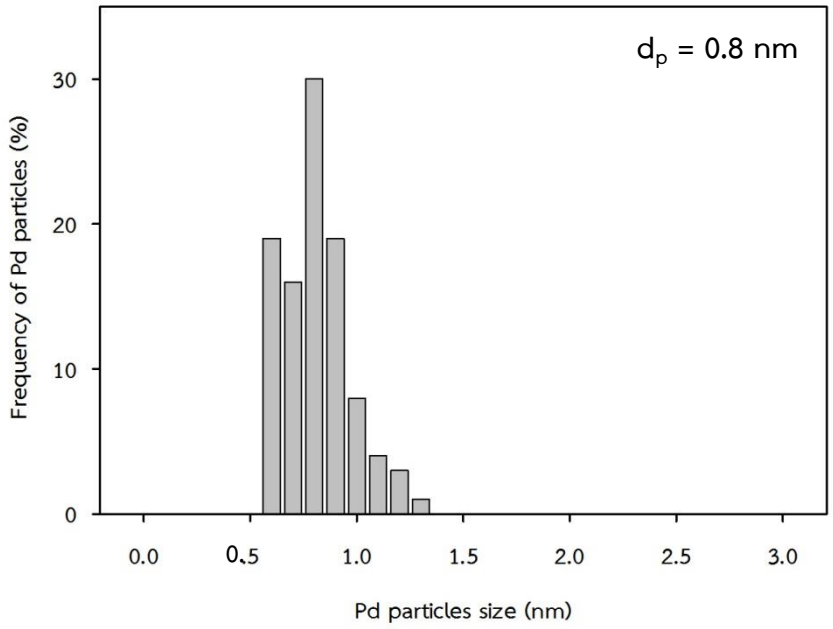

Figure 4.27 Pd particle size distribution of the Pd/N10T300 catalyst

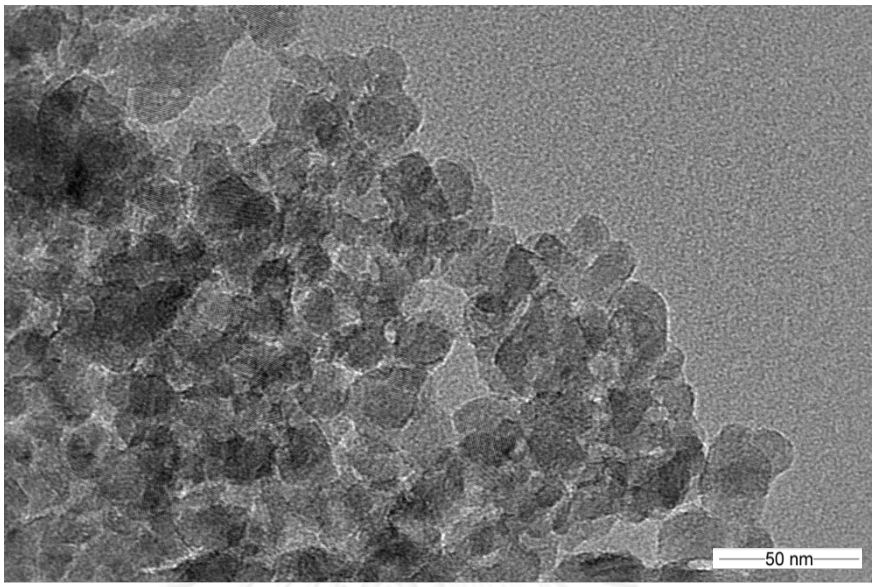

Figure 4.28 TEM images of the Pd/N50T300 catalyst

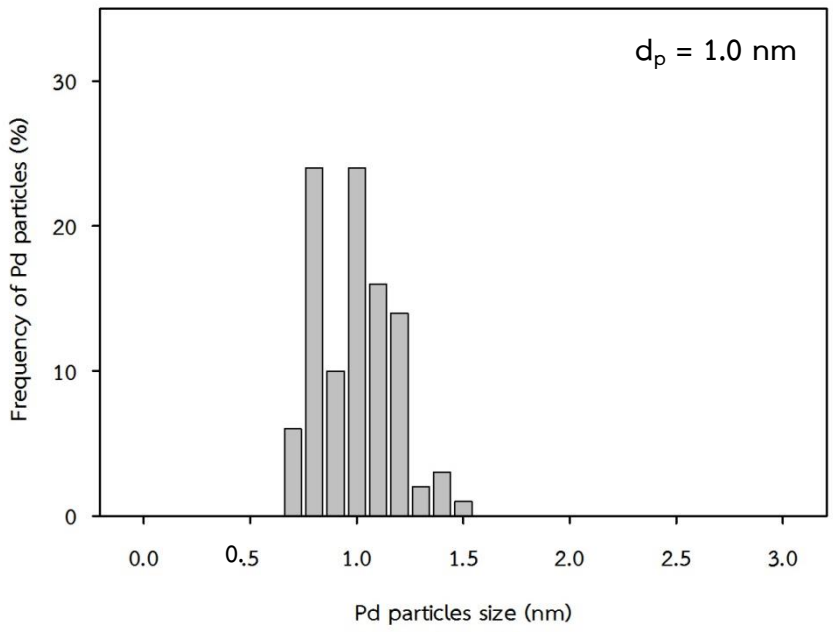

Figure 4.29 Pd particle size distribution of the Pd/N50T300 catalyst

4.2.1.7 H_2 chemisorption

The amounts of H_2 chemisorption of all the catalysts are given in **Table 4.8,** which related to amount of active surface Pd metal on the catalyst samples, %Pd dispersion. The average Pd^{o} particle size was calculated from H_2 consumption. The %Pd dispersion was determine by the stoichiometric factor H/Pd = 1 [69] and the average Pd^{o} particle size was calculated base on : d_p Pd^{o} (nm) = 1.1/D, where D is the fractional metal dispersion [70].

For the Pd catalysts supported on N-doped TiO_2 supports with different amounts of NMP solution and calcination temperature at 300°C suggested that the amounts of H_2 consumption decreased in with increasing amounts of added NMP solution. The Pd active sites were found to decrease in the order Pd/N10T300 > Pd/N15T300 > Pd/N20T300 > Pd/N30T300 > Pd/N50T300, respectively from 3.40×10^{18}-3.18×10^{18} H_2 molecule/g-catalyst, Pd dispersion decreased from 12.01-7.73% and average Pd^{o} particle size increased from 9.16-14.29 nm. The results from H_2 chemisorption suggested that the amounts of H_2 consumption decreased with increasing amounts NMP solution doping. It may be due to some agglomeration of catalysts with increasing amounts of NMP solution.

Table 4.8 The amounts of H_2 consumption of all the catalysts

Sample	H_2 consumption (μL/g-catalyst)	Pd active sites ($\times10^{-18}$ molecule/g-catalyst)	Pd dispersion (%)	d_p Pd^{o} (nm)
Pd/N10T300	63.22	3.40	12.0	9.2
Pd/N15T300	60.88	3.27	11.6	9.5
Pd/N20T300	60.00	3.22	11.4	9.7
Pd/N30T300	59.27	3.18	11.3	9.8
Pd/N50T300	40.68	2.19	7.7	14.3

4.2.2 Catalytic activity

The catalytic activity of the Pd catalysts supported on the N-doped TiO_2 supports with different amounts of NMP solution and calcination temperature at 300^{o}C were evaluated in the liquid phase selective hydrogenation of 1-heptyne. The products of 1-heptene hydrogenation reaction which were detected by a CG after termination of the reaction testing were 1-heptyne (desired product) and n-heptane.

The conversion in the liquid phase hydrogenation of 1-heptyne on the Pd/N10T300, Pd/N15T300, Pd/N20T300, Pd/N30T300 and Pd/N50T300 catalysts are shown in **Figure 4.30.** In this study, the conversion depended on the amounts of Pd active, Pd dispersion and average Pd^{o} particle size. The hydrogenation rate increased in the order Pd/N10T300 > Pd/N15T300 > Pd/N20T300 > Pd/N30T300 > Pd/N50T300. The hydrogenation of 1-heptyne was complete in 60 min for the Pd/N10T300, Pd/N15T300 and Pd/N20T300 catalysts and 120 min for the Pd/N30T300 and Pd/N50T300. The BET surface of Pd catalysts supported on N-doped TiO_2 with different amounts of NMP solution decreased with increasing amounts of added NMP solution. However, the selectivity of heptene at final reaction time was found to be in the order Pd/N20T300 (90.1%) > Pd/N30T300 (87.1%) > Pd/N15T300 (82.9%) > Pd/N50T300 (69.6%) > Pd/N10T300 (65.0%) which are shown in **Figure 4.31.**

The results in this study, For the Pd/N10T300 and Pd/N15T300 catalysts showed the peak shift to higher binding energies correspond to electron-deficient palladium (Pd^{n+}), which are less active as they have less electrons available for interacting with the surface [74]. Therefore, the highest presence of Ti^{3+} of the Pd/N15T300 catalysts did not exhibited the interaction between Pd with TiO_2 support same as the Pd/N10T300 catalyst. The Pd/N20T300 catalyst presented of Ti^{3+} as 7.88%. Reducing the amount of Ti^{3+} as a result of the dislodgement of partially nitrogen atoms. So, the opportunity Pd can be contact with Ti^{3+} on surface TiO_2 has increased, effect on strong interaction between Pd with TiO_2 support resulting in higher selectivity of heptene.

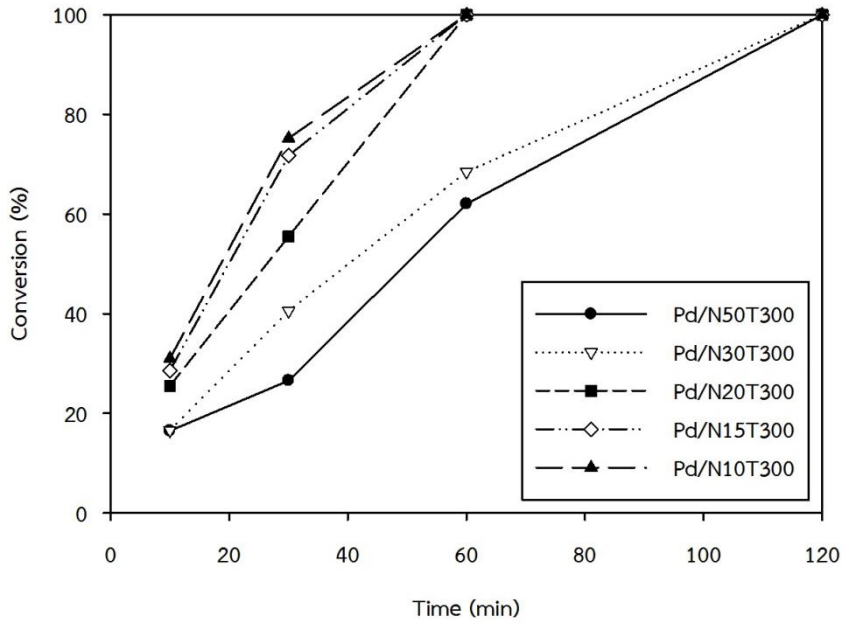

Figure 4.30 Hygrogenation of 1-heptyne on the Pd/N10T300, Pd/N15T300, Pd/N20T300, Pd/N30T300 and Pd/N50T300 catalysts

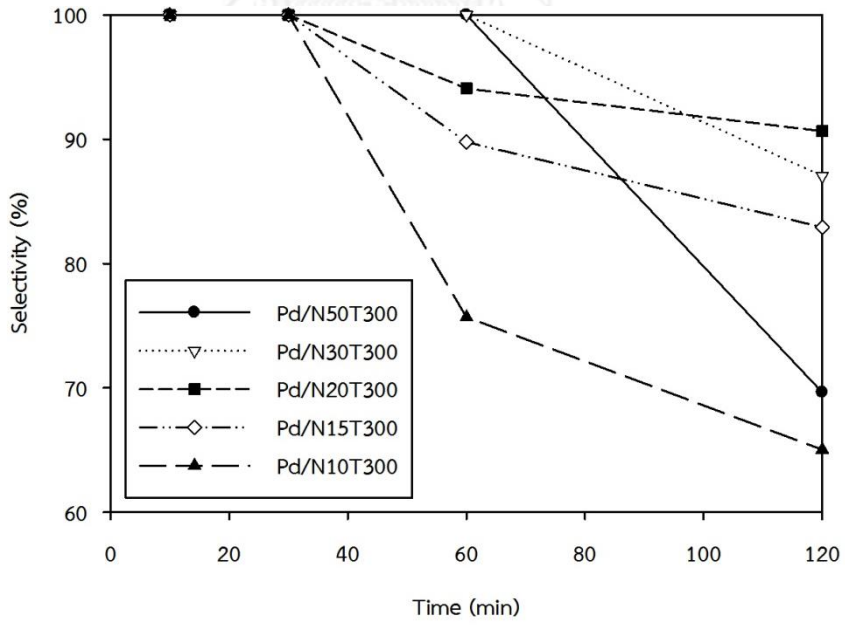

Figure 4.31 Heptene selectivity in hydrogenation of 1-heptyne on the Pd/N10T300, Pd/N15T300, Pd/N20T300, Pd/N30T300 and Pd/N50T300 catalysts

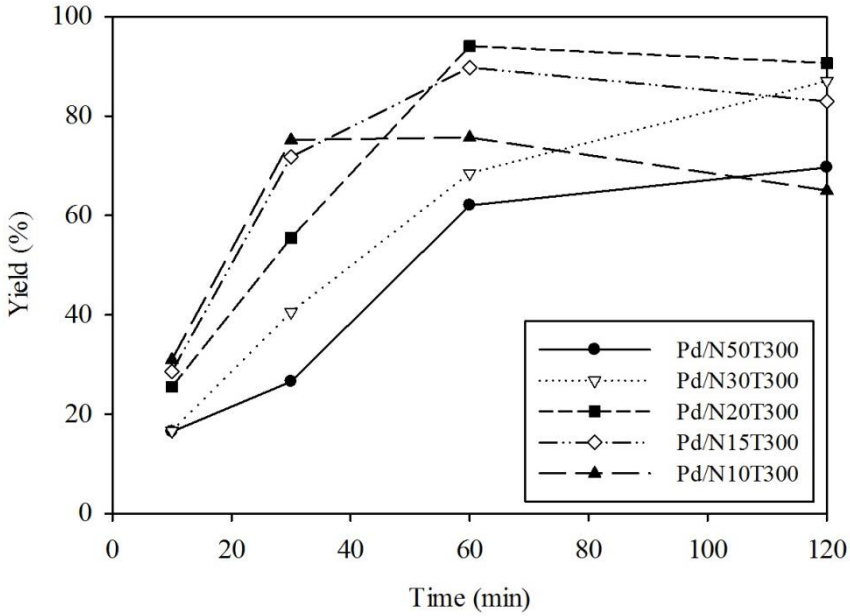

Figure 4.32 Yield of heptene product on the Pd/N10T300, Pd/N15T300, Pd/N20T300, Pd/N30T300 and Pd/N50T300 catalysts

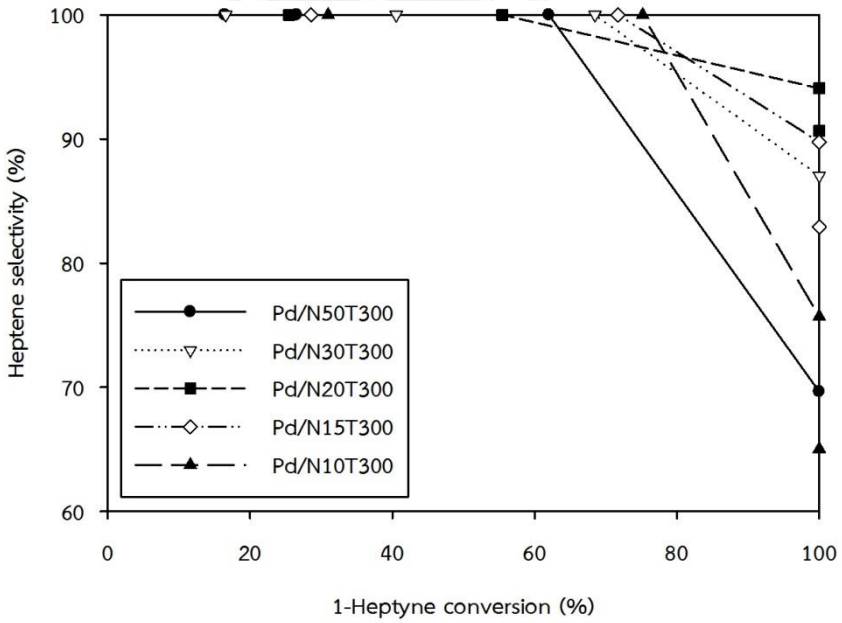

Figure 4.33 The performance of 1-heptyne hydrogenation over the Pd/N10T300, Pd/N15T300, Pd/N20T300, Pd/N30T300 and Pd/N50T300 catalysts

The yield t of heptene produc and the performance plots of 1-heptyne hydrogenation on Pd/N10T300, Pd/N15T300, Pd/N20T300, Pd/N30T300 and Pd/N50T300 are shown in **Figure 4.32** and **Figure 4.33.** The yield of heptene product was found to be in the order Pd/N20T300 (94.1%) at 60 min > Pd/N15T300 (89.8%) at 60 min > Pd/N30T300 (87.1%) at 120 min > Pd/N10T300 (75.5%) at 60 min > Pd/N50T300 (69.6%) at 120 min. The Pd/N20T300 catalyst exhibited best the performance of 1-heptyne hydrogenation with highest heptane yield (~90%) at complete conversion of 1-heptyne.

CHAPTER 5

CONCLUSIONS AND RECOMMENDATIONS

The effects of the calcination and amount of NMP the nitrogen doped TiO_2 supported Pd catalysts were studied in the liquid-phase selective hydrogenation of 1-heptyne to 1-heptene. The following conclusions and recommendations can be drawn :

5.1 Conclusions

Addition of NMP on TiO_2 supports resulted in higher Pd dispersion and hydrogenation activity of Pd/TiO_2 catalyst in the liquid-phase selective hydrogenation of 1-heptyne. Calcination of NMP added TiO_2 at 300°C prior to impregnation of Pd showed better catalytic performance than those prepared without calcination step or calcined at 200°C.

Among the catalysts in this study, the Pd catalysts supported on N-doped TiO_2 supports. The Pd/N20T300 catalyst exhibited the best catalyst performance, in which relatively highest heptene selectivity (~90%) was obtained at complete conversion of 1-heptyne. The improved catalytic performances were attributed to larger surface area, well dispersion of small Pd particles, higher amounts of Pd active sites and stronger metal-support interaction.

It is also proposes that NMP replaced O atoms on the TiO_2 surface so that higher Pd dispersion and stronger interaction of Pd- TiO_2 supports were obtained.

5.2 Recommendations

1) The nitrogen doping using another solution such as NH_3, NH_4NO_3 and NH_4Cl as nitrogen source via the sol-gel method should be studied. It is still unclear about nitrogen atom substitution of oxygen atom in the TiO_2 lattice and/or TiO_2 surface, so further characterization should be carried out.

2) The catalysts could be reduced at higher temperature (~500°C) in order investigate the effect of strong metal support interaction (SMSI) on the catalytic behavior of the Pd/N-doped TiO_2 catalyst comparing to the Pd/TiO_2 catalyst in the liquid phase selective hydrogenation of alkyne to alkene.

3) The nitrogen doping on titania supports may be affected on interaction between Pd and TiO_2 supports so it is interesting to study the ability in reduction using H_2-TPR technique.

REFERENCES

[1] Semagina, N. and Kiwi-Minsker, L. Recent Advances in the Liquid-Phase Synthesis of Metal Nanostructures with Controlled Shape and Size for Catalysis. Catalysis Reviews 51(2) (2009): 147-217.

[2] Árpád Molnár, A.S., Mónika Vargaa. Hydrogenation of carbon–carbon multiple bonds: chemo-, regio- and stereo-selectivity. Journal of Molecular Catalysis A: Chemical 332 (2010): 106-112.

[3] László Guczi, A.H., Andrea Beck, Antal Sárkány. 75 Controlling metal particle size in preparation of Pd/SiO_2 catalysts. Studies in Surface Science and Catalysis: Science and Technology 145 (2003): 351-354.

[4] Olgioly Dom´ınguez-Quintero, Susana Mart´ınez, Yurgenis Henr´ıquez, Lindora D'Ornelas, Heinz Krentzien, and Osuna, J. Silica-supported palladium nanoparticles show remarkable hydrogenation catalytic activity. Journal of Molecular Catalysis A: Chemical 197 (2003): 185-191.

[5] Weerachawanasak, P., Praserthdam, P., Arai, M., and Panpranot, J. A comparative study of strong metal–support interaction and catalytic behavior of Pd catalysts supported on micron- and nano-sized TiO_2 in liquid-phase selective hydrogenation of phenylacetylene. Journal of Molecular Catalysis A: Chemical 279(1) (2008): 133-139.

[6] Árpád Molnár, Antal Sárkány, and Varga, M. Hydrogenation of carbon–carbon multiple bonds: chemo-, regio- and stereo-selectivity. Journal of Molecular Catalysis A: Chemical 173(1-2) (2001): 185-221.

[7] Panpranot, J., Phandinthong, K., Praserthdam, P., Hasegawa, M., Fujita, S.-i., and Arai, M. A comparative study of liquid-phase hydrogenation on Pd/SiO_2 in organic solvents and under pressurized carbon dioxide: Activity change and metal leaching/sintering. Journal of Molecular Catalysis A: Chemical 253(1-2) (2006): 20-24.

[8] Azizi, Y., Petit, C., and Pitchon, V. Formation of polymer-grade ethylene by selective hydrogenation of acetylene over Au/CeO_2 catalyst. Journal of Catalysis 256(2) (2008): 338-344.

[9] Lopez-Sanchez, J.A. and Lennon, D. The use of titania- and iron oxide-supported gold catalysts for the hydrogenation of propyne. Applied Catalysis A: General 291(1-2) (2005): 230-237.

[10] Mitsutaka Okumura, Tomoki Akita, and Haruta, M. Hydrogenation of 1,3-butadiene and of crotonaldehyde over highly dispersed Au catalysts. Catalysis Today 74 (2002): 265-269.

[11] Zhang, X., Shi, H., and Xu, B.-Q. Comparative study of Au/ZrO_2 catalysts in CO oxidation and 1,3-butadiene hydrogenation. Catalysis Today 122(3-4) (2007): 330-337.

[12] Nikolaev, S.A. and Smirnov, V.V. Synergistic and size effects in selective hydrogenation of alkynes on gold nanocomposites. Catalysis Today 147 (2009): S336-S341.

[13] Campo, B., Volpe, M., Ivanova, S., and Touroude, R. Selective hydrogenation of crotonaldehyde on $Au/HSA-CeO_2$ catalysts. Journal of Catalysis 242(1) (2006): 162-171.

[14] James M. Kerr, Colin J. Suckling, and Bamfield, P. Selective hydrogenation by a novel palladium(II) complex. Tetrahedron Letters 29(43) (1988): 5545-5548.

[15] P.C. L'Argentière, E.A. Cagnola, M.E. Quiroga, and Liprandi, D.A. A palladium tetra-coordinated complex as catalyst in the selective hydrogenation of 1-heptyne. Applied Catalysis A: General 226 (2002): 253-263.

[16] An, K., Musselwhite, N., Kennedy, G., Pushkarev, V.V., Baker, L.R., and Somorjai, G.A. Preparation of mesoporous oxides and their support effects on Pt nanoparticle catalysts in catalytic hydrogenation of furfural. J Colloid Interface Sci 392 (2013): 122-8.

[17] Ekou, T., et al. Citral hydrogenation over Rh and Pt catalysts supported on TiO_2: Influence of the preparation and activation protocols of the catalysts. Journal of Molecular Catalysis A: Chemical 337(1-2) (2011): 82-88.

[18] Ekou, T., Vicente, A., Lafaye, G., Especel, C., and Marecot, P. Bimetallic Rh-Ge and Pt-Ge catalysts supported on TiO_2 for citral hydrogenation. Applied Catalysis A: General 314(1) (2006): 64-72.

[19] Álvarez-Rodríguez, J., Rodríguez-Ramos, I., Guerrero-Ruiz, A., Gallegos-Suarez, E., and Arcoya, A. Influence of the nature of support on Ru-supported catalysts for selective hydrogenation of citral. Chemical Engineering Journal 204-206 (2012): 169-178.

[20] McArdle, S., Girish, S., Leahy, J.J., and Curtin, T. Selective hydrogenation of sunflower oil over noble metal catalysts. Journal of Molecular Catalysis A: Chemical 351 (2011): 179-187.

[21] Westerterp, A.N.R.B.a.K.R. Mechanism and kinetics of the selective hydrogenation of ethyne and ethene Chemical Engineering and Processing 36 (1997): 1-7.

[22] Maccarrone, M.J., et al. Partial hydrogenation of 3-hexyne over low-loaded palladium mono and bimetallic catalysts. Applied Catalysis A: General 441-442 (2012): 90-98.

[23] Tatsuhiro Nozoe, et al. Non-solvent hydrogenation of solid alkenes and alkynes with supported palladium catalysts. Solid State Ionics 141-142 (2001): 695-700.

[24] García-Mota, M., Bridier, B., Pérez-Ramírez, J., and López, N. Interplay between carbon monoxide, hydrides, and carbides in selective alkyne hydrogenation on palladium. Journal of Catalysis 273(2) (2010): 92-102.

[25] Tew, M.W., Janousch, M., Huthwelker, T., and van Bokhoven, J.A. The roles of carbide and hydride in oxide-supported palladium nanoparticles for alkyne hydrogenation. Journal of Catalysis 283(1) (2011): 45-54.

[26] Kittisakmontree, P., Pongthawornsakun, B., Yoshida, H., Fujita, S.-i., Arai, M., and Panpranot, J. The liquid-phase hydrogenation of 1-heptyne over Pd–Au/TiO_2 catalysts prepared by the combination of incipient wetness impregnation and deposition–precipitation. Journal of Catalysis 297 (2013): 155-164.

[27] Dal Santo, V., Gallo, A., Naldoni, A., and Sordelli, L. Selective butadiene hydrogenation by Pd nanoparticles deposed onto nano-sized oxide supports by CVD of Pd-hexafluoroacetylacetonate. Inorganica Chimica Acta 380 (2012): 216-222.

[28] T.A. Nijhuis, G. van Koten, and Moulijn, J.A. Optimized palladium catalyst systems for the selective liquid-phase hydrogenation of functionalyzed alkynes. Applied Catalysis A: General 238 (2003): 259-271.

[29] Teschner, D., et al. Alkyne hydrogenation over Pd catalysts: A new paradigm. Journal of Catalysis 242(1) (2006): 26-37.

[30] Quiroga, M.E., Liprandi, D.A., Cagnola, E.A., and L' Argentière, P.C. 1-Heptyne semihydrogenation catalized by palladium or rhodium complexes. Applied Catalysis A: General 326(2) (2007): 121-129.

[31] Kang, J. Selective Hydrogenation of Acetylene on TiO_2-Added Pd Catalysts. Journal of Catalysis 208(2) (2002): 310-320.

[32] Li, Y., et al. The effect of titania polymorph on the strong metal-support interaction of Pd/TiO_2 catalysts and their application in the liquid phase selective hydrogenation of long chain alkadienes. Journal of Molecular Catalysis A: Chemical 216(1) (2004): 107-114.

[33] Gandhe, A.R. and Fernandes, J.B. A simple method to synthesize N-doped rutile titania with enhanced photocatalytic activity in sunlight. Journal of Solid State Chemistry 178(9) (2005): 2953-2957.

[34] Kaewgun, S., Nolph, C.A., Lee, B.I., and Wang, L.-Q. Influence of hydroxyl contents on photocatalytic activities of polymorphic titania nanoparticles. Materials Chemistry and Physics 114(1) (2009): 439-445.

[35] Kačer, P., Spurná, P., and Červený, L. Coadsorption effect of the alkenic bond on the hydrogenation of the alkynic substrate on platinum and palladium catalysts. Journal of Molecular Catalysis A: Chemical 202(1-2) (2003): 269-277.

[36] Ibragimov, V.A. CATALYSIS. Thermopedia (2011).

[37] Carey, F.A. Organic Chemistry 4th Edition ed. McGraw-Hill College: McGraw-Hill College, Boston, MA, 2000.

[38] Hans-Ulrich Blaser, A.I., Anita Schnyder, Heinz Steiner, Martin Studer. Supported palladium catalysts for fine chemicals synthesis. Journal of Molecular Catalysis A: Chemical 173(1-2) (2001): 3-18.

[39] Colmenares, J.C., et al. Influence of the strong metal support interaction effect (SMSI) of Pt/TiO_2 and Pd/TiO_2 systems in the photocatalytic biohydrogen production from glucose solution. Catalysis Communications 16(1) (2011): 1-6.

[40] Mekasuwandumrong, O., Phothakwanpracha, S., Jongsomjit, B., Shotipruk, A., and Panpranot, J. Liquid-Phase Selective Hydrogenation of 1-Heptyne over Pd/TiO_2 Catalyst Synthesized by One-Step Flame Spray Pyrolysis. Catalysis Letters 136(1-2) (2010): 164-170.

[41] C. Kemball, D.A.D., G. J. K. Acres, A. J. Bird, J. W. Jenkins and F. King The design and preparation of supported catalysts. 1981.

[42] Alireza Khataee, G.A.M. Nanostructure Titanium Dioxide Meterials: Properties, Preparation and Applications. World Scientific Publishing Co. Pte. Ltd., 2012.

[43] Kazuhito HASHIMOTO, H.I.a.A.F. TiO2 Photocatalysis: A Historical Overview and Future Prospects. Japanese Journal of Applied Physics 44 (2005): 8269-8285.

[44] Akira Fujishima, T.N.R., Donald A. Tryk. Titanium dioxide photocatalysis. Journal of Photochemistry and Photobiology C: Photochemistry Reviews 1(1) (2000): 1-21.

[45] Nolan, N., Pillai, S., Seery, M. Spectroscopic Investigation of the Anatase-to-Rutile Transformation of Sol-Gel Synthesised TiO_2 Photocatalysts. Journal of Physical Chemistry C 113 (2009): 16151-16157.

[46] Yi Hu, H.-L.T., C.-L. Huang. Effect of brookite phase on the anatase–rutile transition in titania nanoparticles. Journal of the European Ceramic Society 23(5) (2003): 691-696.

[47] Reyes-Coronado, D., Rodriguez-Gattorno, G., Espinosa-Pesqueira, M.E., Cab, C., de Coss, R., and Oskam, G. Phase-pure TiO_2 nanoparticles: anatase, brookite and rutile. Nanotechnology 19(14) (2008): 145605.

[48] Luo, H., Wang, C., and Yan, Y. Synthesis of Mesostructured Titania with Controlled Crystalline Framework. Chemistry of Materials 15(20) (2003): 3841-3846.

[49] Sugimoto, T., Zhou, X., and Muramatsu, A. Synthesis of uniform anatase TiO_2 nanoparticles by gel–sol method. J Colloid Interface Sci 259(1) (2003): 43-52.

[50] Scherer, C.J.B.a.G.W. Sol-Gel Science: The Physics and Chemistry of Sol-Gel Processing. 1 ed. Elsevier Science (USA), 1990.

[51] Hung, W.C., Fu, S.H., Tseng, J.J., Chu, H., and Ko, T.H. Study on photocatalytic degradation of gaseous dichloromethane using pure and iron ion-doped TiO_2 prepared by the sol-gel method. Chemosphere 66(11) (2007): 2142-51.

[52] M. Niederberger, M.H.B., G. D. Stucky. Benzyl Alcohol and Titanium TetrachlorideA Versatile Reaction System for the Nonaqueous and Low-Temperature Preparation of Crystalline and Luminescent Titania Nanoparticles. Chemistry of Materials 14(10) (2002): 4364-4370.

[53] Jiang, X., Herricks, T., and Xia, Y. Monodispersed Spherical Colloids of Titania: Synthesis, Characterization, and Crystallization. Advanced Materials 15(14) (2003): 1205-1209.

[54] Wang, C.-C. and Ying, J.Y. Sol–Gel Synthesis and Hydrothermal Processing of Anatase and Rutile Titania Nanocrystals. Chemistry of Materials 11(11) (1999): 3113-3120.

[55] Venkatachalam, N., Palanichamy, M., and Murugesan, V. Sol–gel preparation and characterization of nanosize TiO_2: Its photocatalytic performance. Materials Chemistry and Physics 104(2-3) (2007): 454-459.

[56] Pelaez, M., et al. A review on the visible light active titanium dioxide photocatalysts for environmental applications. Applied Catalysis B: Environmental 125 (2012): 331-349.

[57] Sato, S. Photocatalytic activity of NO_x-doped TiO_2 in the visible light region. Chemical Physics Letters 123(1-2) (1986): 126-128.

[58] Nosaka, Y., Matsushita, M., Nishino, J., and Nosaka, A.Y. Nitrogen-doped titanium dioxide photocatalysts for visible response prepared by using organic compounds. Science and Technology of Advanced Materials 6(2) (2005): 143-148.

[59] Qin, H.-L., Gu, G.-B., and Liu, S. Preparation of nitrogen-doped titania with visible-light activity and its application. Comptes Rendus Chimie 11(1-2) (2008): 95-100.

[60] Di Valentin, C., et al. N-doped TiO_2: Theory and experiment. Chemical Physics 339(1-3) (2007): 44-56.

[61] Wu, H., Ma, J., Zhang, C., and He, H. Effect of TiO2 calcination temperature on the photocatalytic oxidation of gaseous NH_3. Journal of Environmental Sciences 26(3) (2014): 673-682.

[62] Sing, K.S.W. Reporting physisorption data for gas/solid systems with special reference to the determination of surface area and porosity (Recommendations 1984). Pure and Applied Chemistry 57(4) (1985).

[63] Kim, K.S., Gossmann, A.F., and Winograd, N. X-ray photoelectron spectroscopic studies of palladium oxides and the palladium-oxygen electrode. Analytical Chemistry 46(2) (1974): 197-200.

[64] Linsmeier, C. and Taglauer, E. Strong metal–support interactions on rhodium model catalysts. Applied Catalysis A: General 391(1-2) (2011): 175-186.

[65] Viswanathan, B. Photocatalytic processes – Selection Criteria for the Choice of Materials Catalysis Society of India 2 (2003): 71-74.

[66] Li, Y., Ma, G., Peng, S., Lu, G., and Li, S. Boron and nitrogen co-doped titania with enhanced visible-light photocatalytic activity for hydrogen evolution. Applied Surface Science 254(21) (2008): 6831-6836.

[67] Socrates, G. Infrared and Raman Characteristic Group Frequencies: Tables and Charts. 3rd Edition ed.: Wiley, 2001.

[68] Jyoti Yadav, N., S., Pandeya, Gopal Nath, and Singh, S.P. Synthesis and antibacterial evaluation of some hydrazones of flavanoid derivatives. Journal of Chemical and Pharmaceutical Research 2(4) (2010): 558-563.

[69] Amorim, C. and Keane, M.A. Palladium supported on structured and nonstructured carbon: A consideration of Pd particle size and the nature of reactive hydrogen. J Colloid Interface Sci 322(1) (2008): 196-208.

[70] Nishikiori, H., Hayashibe, M., and Fujii, T. Visible Light-Photocatalytic Activity of Sulfate-Doped Titanium Dioxide Prepared by the Sol–Gel Method. Catalysts 3(2) (2013): 363-377.

[71] Lim, J., et al. Synergic photocatalytic effects of nitrogen and niobium co-doping in TiO_2 for the redox conversion of aquatic pollutants under visible light. Journal of Catalysis 310 (2014): 91-99.

[72] Cheng, P., Qiu, J., Gu, M., Jin, Y., and Shangguan, W. Synthesis of shape-controlled titania particles from a precursor solution containing urea. Materials Letters 58(29) (2004): 3751-3755.

[73] Cheng, P., Deng, C., Gu, M., and Dai, X. Effect of urea on the photoactivity of titania powder prepared by sol–gel method. Materials Chemistry and Physics 107 (2008): 77-81.

[74] Badano, J., Lederhos, C., and L'Argentière, M.Q.y.P. Low metal loading catalysts used for the selective hydrogenation of styrene. Artigo 33(1) (2010): 48-51.

APPENDIX

APPENDIX A

Determination for all the catalysts preparation

The chemical used for all the catalysts preparation of 0.5wt%Pd.

- Palladium (II) chloride 99.99% ($PdCl_2$), Aldrich
- Hydrochloric acid 37% (HCl), QRëC

Determination for all the catalysts preparation of 0.5wt%Pd by using wet impregnation method. Based on 100 g of catalyst used :

Palladium = 0.5 g

Then, Support = (100 – 0.5) g

So, Support = 99.5 g

For Support = 1 g

Then, Palladium required in grams = $\frac{(1\,g)\times(0.5\,g)}{(99.5\,g)}$

So, Palladium required in grams = 5.021×10^{-3} g

Palladium (II) chloride that used as the precursor:

M.W. $PdCl_2$ (99.99%) = 177.326 g/mol

M.W. Pd = 106.421 g/mol

Then, Palladium (II) chloride required in grams = $\frac{(5.0251\times10^{-3}\,g)\times(177.149\,g/mol)}{(106.421\,g/mol)}$

So, Palladium (II) chloride required in grams = 5.021×10^{-3} g

APPENDIX B

Determination for H_2 chemisorption

Determination for amounts H_2 consumption, Pd active sites, Pd dispertion and average Pd metal particle size are defined as follow :

Volume of active gas dosed from a loop

$$V_{inj} = \frac{T_{std}}{T_{amb}} \times \frac{P_{atm}}{P_{std}} \times \frac{A\,(\%)}{100\,\%} \times V_{loop}$$

Where V_{inj} = volume of active gas dosed from a loop

V_{loop} = loop volume injected

T_{std} = standard temperature

T_{atm} = ambient temperature

P_{std} = standard pressure

P_{atm} = ambient pressure

A (%) = % active gas

When V_{loop} = 100 µl

T_{std} = 273 K

T_{atm} = 295 K

P_{std} = 760 mmHg

P_{atm} = 743 mmHg

A (%) = 100 %

Then, $$V_{inj} = \frac{273\,K}{295\,K} \times \frac{743\,mmHg}{760\,mmHg} \times \frac{100\,\%}{100\,\%} \times 100\,\mu l$$

So, V_{inj} = 90.4723 µl

Volume chemisorbed

$$V_{ads} = \frac{V_{inj}}{M} \times \sum_{i=1}^{n} \left(1 - \frac{A_i}{A_f} \right)$$

Where V_{ads} = volume of chemisorbed

V_{inj} = volume of active gas dosed from a loop

M = mass of sample

A_f = area of peak last peak

A_i = any area of peak previous last peak

i = start at this value

n = go to this value

For example : Pd/N10T300

Where V_{inj} = 90.4723 µl

M = 1.005 g

i = 1

n = 4

No. peak	A_i	$\frac{A_i}{A_f}$	$1 - \frac{A_i}{A_f}$
1	0.01449	0.039682	0.690318
2	0.04636	0.990810	0.009190
3	0.04666	0.997222	0.002778
4	0.04679	1	0
Sum			0.702287

$$\sum_{i=1}^{4}\left(1-\frac{A_i}{A_f}\right) = 0.702287$$

Then, $$V_{ads} = \frac{90.7423\mu l}{1.005 g} \times 0.702287$$

So, $$V_{ads} = 63.2214 \mu l/g\text{-catalyst}$$

Converts from μl/g-catalyst unit to molecule/g-catalyst unit :

Where V_{ads} = volume of chemisorbed

T_{ads} = adsorption temperature

P = pressure standard

R = gas contant

When V_{ads} = 63.2214 μl/g-catalyst = 6.32214×10^{-5} l/g-catalyst

T_{ads} = 302.35 K

P = 1 atm

R = 0.08206 (L·atm)/(K·mol)

Then, $$V_{ads} = \frac{6.32214\times 10^{-5}\ l/g\text{-catalyst}}{0.08206(L\cdot atm)/(K\cdot mol)} \times \frac{1\,atm}{302.35K}$$

$$V_{ads} = 2.5481\times 10^{-5} mol/g\text{-catalyst}$$

Used the formula :

$$n = \frac{N}{N_A}$$

Where n = mole

N = molecule

N_A = Avogadro's number

When $n = 2.5481 \times 10^{-5}$ mol/g - catalyst

$N_A = 6.02 \times 10^{23}$ molecules/mole

So, $N = (6.02 \times 10^{23} \text{ molecules/mole}) \cdot (2.5481 \times 10^{-5} \text{ mol/g - catalyst})$

$N = (1.5340 \times 10^{18} \text{ molecules/g - catalyst})$

Pd active sites

Used the formula :

$$\text{Pd active sites} = S_f \times N_A \times \frac{V_{ads}}{V_g}$$

Where S_f = stoichiometry factor

N_A = Avogadro's number

V_{ads} = volume of chemisorbed

V_g = molar volume of gas at STP

When S_f = 2

N_A = 6.02×10^{23} molecules/mole

V_{ads} = 6.32214×10^{-5} l/g-catalyst

V_g = 22.414 L/mole

Then, $$\text{Pd active sites} = 2 \times 6.02 \times 10^{23} \text{ molecules/mole} \times \frac{6.32214 \times 10^{-5} \text{ l/g - catalyst}}{22.414 \text{ L/mole}}$$

So, $\text{Pd active sites} = 3.3960 \times 10^{18}$ molecules/g - catalyst

% Pd metal dispersion

Used the formula :

$$\%D = S_f \times \frac{V_{ads}}{V_g} \times \frac{M.W.}{\%M} \times 100\% \times 100\%$$

Where $\%D$ = % Pd metal dispersion

S_f = stoichiometry factor

V_{ads} = volume of chemisorbed

V_g = molar volume of gas at STP

M.W. = molecular weight of palladium

$\%M$ = weight percent palladium loading

When S_f = 2

V_{ads} = 6.32214×10^{-5} l/g-catalyst

V_g = 22.414 L/mole

M.W. = 106.42 g/mole

$\%M$ = 0.5 %

Then, $$\%D = 2 \times \frac{6.32214 \times 10^{-5}\ l/g\text{-catalyst}}{22.414 L/mole} \times \frac{106.45 g/mole}{0.5\%} \times 100\% \times 100\%$$

So, $\%D = 12.0068\%$

Pd Metal particles size

Used the formula :

$$d_pPd^{o} = \frac{1.1}{D}$$

Where d_pPd^{o} = Pd metal particles size (nm)

D = fractional metal dispersion

When D = 0.120068

Then, $d_pPd^{o} = \frac{1.1}{0.120068}$

So, $d_pPd^{o} = 9.1615nm$

APPENDIX C

Determination for the conversion and selectivity

Determination for the conversion of 1-heptyne and the selectivity of heptane are defined as follow :

$$\% \text{ Conversion of 1 - heptyne} = \frac{(1 - \text{heptyne feed}) - (1 - \text{heptyne in product})}{1 - \text{heptyne in feed}} \times 100$$

$$\% \text{ Selectivity of heptene} = \frac{(\text{heptene in product}) - (\text{heptene in feed})}{(1 - \text{heptyne in feed}) - (1 - \text{heptyne in product})} \times 100$$

VITA

Miss Siwaporn Phetthongchuai was born on 17 October 1987, in Nakhonsithammarat, Thailand. She received her Bachelor degree of Chemical Engineering from Rajamangala University of Technology Thanyaburi, Thailand in March 2010. Since May 22, 2012, she has been studying for her Master degree of Engineering from the department of Chemical Engineering, Chulalongkorn University.

List of publication :

Siwaporn Phetthongchuai and Joongjai Panpranot, “Characteristics and Catalytic Properties of Pd Catalysts Supported on N-doped TiO2 in the Selective Hydrogenation of 1-Heptyne”, Proceeding of the 3rd international Thai Chemical Engineering and Applied Chemistry Conference, Khon Kaen, Thailand, October 17-18, 2013.